There are relatively few reports about the regulation of SXR expression to date. Aouabdi *et al.* (2006) reported the presence of a PPAR alpha binding site 2.2 kb upstream of the transcription start site in human SXR. This site corresponded to the induction site with clofibrate in the rat and they further confirmed its importance using human liver cancer cell line (Huh7). Jung *et al.* (2006) reported the presence of four FXR binding sites in intron 2 of the mouse SXR gene that were required for FXR regulation of SXR expression. This intron 2 region is completely intact in our hSXRki mouse. Therefore, the regulation by FXR should be preserved in our mice.

Compared to the previously generated humanized Alb-SXR, SXR BAC, and hSXR genome mice, we contend that our hSXRki mouse has an advantage because the human-mouse chimeric gene is expressed in the same tissues and at similar levels to endogenous SXR in WT mice under control of the mouse promoter. This feature would make this model suitable not only for systemic toxicity but also toxicity at various stages of development of the embryo and fetus, maturation of infant, and of senescence, where the *cis* and *trans* regulations might be critical in its regulation (Sarsero *et al.,* 2004) (Konopka *et al.,* 2009). Thus, we believe that our system has a broader application range for toxicological studies.

ACKNOWLEDGMENTS

The authors thank Ms. Yuko Matsushima, Mr. Masaki Tsuji, Ms. Maki Otsuka, Mr. Yusuke Furukawa, Mr. Kouichi Morita, Ms. Maki Abe, and Ms. Shinobu Watanabe for technical support. This study was supported in part by the Health Sciences Research Grants H19-Toxico-Shitei-001 from the Ministry of Health, Labour and Welfare, Japan.

REFERENCES

Aouabdi, S., Gibson, G. and Plant, N. (2006): Transcriptional regulation of the PXR gene: identification and characterization of a functional peroxisome proliferator-activated receptor alpha binding site within the proximal promoter of PXR. Drug Metab. Dispos., **34**, 138-144.

Bertilsson, G., Heidrich, J., Svensson, K., Asman, M., Jendeberg, L., Sydow-Bäckman, M., Ohlsson, R., Postlind, H., Blomquist, P. and Berkenstam, A. (1998): Identification of a human nuclear receptor defines a new signaling pathway for CYP3A induction. Proc. Natl. Acad. Sci., USA, **95**, 12208-12213.

Blumberg, B., Sabbagh, W.Jr., Juguilon, H., Bolado, J.Jr., van Meter, C.M., Ong, E.S. and Evans, R.M. (1998): SXR, a novel steroid and xenobiotic-sensing nuclear receptor. Genes. Dev., **12**, 3195-3205.

Jung, D., Mangelsdorf, D.J. and Meyer, U.A. (2006): Pregnane X receptor is a target of farnesoid X receptor. J. Biol. Chem., **281**, 19081-19091.

Kanno, J., Aisaki, K., Igarashi, K., Nakatsu, N., Ono, A., Kodama, Y. and Nagao, T. (2006): "Per cell" normalization method for mRNA measurement by quantitative PCR and microarrays. BMC genomics, **7**, 64.

Konopka, G., Bomar, J.M., Winden, K., Coppola, G., Jonsson, Z.O., Gao, F., Peng, S., Preuss, T.M., Wohlschlegel, J.A. and Geschwind, D.H. (2009): Human-specific transcriptional regulation of CNS development genes by FOXP2. Nature, **462**, 213-217.

Lehmann, J.M., McKee, D.D., Watson, M.A., Willson, T.M., Moore, J.T. and Kliewer, S.A. (1998): The human orphan nuclear receptor PXR is activated by compounds that regulate CYP3A4 gene expression and cause drug interactions. J. Clin. Invest., **102**, 1016-1023.

Ma, X., Shah, Y., Cheung, C., Guo, G.L., Feigenbaum, L., Krausz, K.W., Idle, J.R. and Gonzalez, F.J. (2007): The PREgnane X receptor gene-humanized mouse: a model for investigating drug-drug interactions mediated by cytochromes P450 3A. Drug Metab. Dispos., **35**, 194-200.

Saga, Y., Hata, N., Koseki, H. and Taketo, M.M. (1997): Mesp2: a novel mouse gene expressed in the presegmented mesoderm and essential for segmentation initiation. Genes. Dev., **11**, 1827-1839.

Saga, Y., Miyagawa-Tomita, S., Takagi, A., Kitajima, S., Miyazaki, J. and Inoue, T. (1999): MesP1 is expressed in the heart precursor cells and required for the formation of a single heart tube. Development, **126**, 3437-3447.

Sakai, K. and Miyazaki, J. (1997): A transgenic mouse line that retains Cre recombinase activity in mature oocytes irrespective of the cre transgene transmission. Biochem. Biophys. Res. Commun., **237**, 318-324.

Sarsero, J.P., Li, L., Holloway, T.P., Voullaire, L., Gazeas, S., Fowler, K.J., Kirby, D.M., Thorburn, D.R., Galle, A., Cheema, S., Koenig, M., Williamson, R. and Ioannou, P.A. (2004): Human BAC-mediated rescue of the Friedreich ataxia knockout mutation in transgenic mice. Mamm. Genome., **15**, 370-382.

Scheer, N., Ross, J., Rode, A., Zevnik, B., Niehaves, S., Faust, N. and Wolf, C.R. (2008): A novel panel of mouse models to evaluate the role of human pregnane X receptor and constitutive androstane receptor in drug response. J. Clin. Invest., **118**, 3228-3239.

Suzuki, T., Akimoto, M., Mandai, M., Takahashi, M. and Yoshimura, N. (2005): A new PCR-based approach for the preparation of RNA probe. J. Biochem. Biophys. Methods., **62**, 251-258.

Tirona, R.G., Leake, B.F., Podust, L.M. and Kim, R.B. (2004): Identification of amino acids in rat pregnane X receptor that determine species-specific activation. Mol. Pharmacol., **65**, 36-44.

Watkins, R.E., Wisely, G.B., Moore, L.B., Collins, J.L., Lambert, M.H., Williams, S.P., Willson, T.M., Kliewer, S.A. and Redinbo, M.R. (2001): The human nuclear xenobiotic receptor PXR: structural determinants of directed promiscuity. Science, **292**, 2329-2333.

Xie, W., Barwick, J.L., Downes, M., Blumberg, B., Simon, C.M., Nelson, M.C., Neuschwander-Tetri, B.A., Brunt, E.M., Guzelian, P.S. and Evans, R.M. (2000): Humanized xenobiotic response in mice expressing nuclear receptor SXR. Nature, **406**, 435-439.

Yagi, T., Tokunaga, T., Furuta, Y., Nada, S., Yoshida, M., Tsukada, T., Saga, Y., Takeda, N., Ikawa, Y. and Aizawa, S. (1993): A novel ES cell line, TT2, with high germline-differentiating potency. Anal. Biochem., **214**, 70-76.

Zhou, C., Tabb, M.M., Sadatrafiei, A., Grün, F. and Blumberg, B. (2004) Tocotrienols activate the steroid and xenobiotic receptor, SXR, and selectively regulate expression of its target genes. Drug Metab. Dispos., **32**, 1075-1082.

LETTER

doi:10.1038/nature10656

GlcNAcylation of histone H2B facilitates its monoubiquitination

Ryoji Fujiki[1], Waka Hashiba[1], Hiroki Sekine[1], Atsushi Yokoyama[1], Toshihiro Chikanishi[1], Saya Ito[1], Yuuki Imai[1], Jaehoon Kim[2], Housheng Hansen He[3], Katsuhide Igarashi[4], Jun Kanno[4], Fumiaki Ohtake[1], Hirochika Kitagawa[1], Robert G. Roeder[2], Myles Brown[3] & Shigeaki Kato[1,5]

Chromatin reorganization is governed by multiple post-translational modifications of chromosomal proteins and DNA[1,2]. These histone modifications are reversible, dynamic events that can regulate DNA-driven cellular processes[3,4]. However, the molecular mechanisms that coordinate histone modification patterns remain largely unknown. In metazoans, reversible protein modification by *O*-linked *N*-acetylglucosamine (GlcNAc) is catalysed by two enzymes, *O*-GlcNAc transferase (OGT) and *O*-GlcNAcase (OGA)[5,6]. However, the significance of GlcNAcylation in chromatin reorganization remains elusive. Here we report that histone H2B is GlcNAcylated at residue S112 by OGT *in vitro* and in living cells. Histone GlcNAcylation fluctuated in response to extracellular glucose through the hexosamine biosynthesis pathway (HBP)[5,6]. H2B S112 GlcNAcylation promotes K120 monoubiquitination, in which the GlcNAc moiety can serve as an anchor for a histone H2B ubiquitin ligase. H2B S112 GlcNAc was localized to euchromatic areas on fly polytene chromosomes. In a genome-wide analysis, H2B S112 GlcNAcylation sites were observed widely distributed over chromosomes including transcribed gene loci, with some sites co-localizing with H2B K120 monoubiquitination. These findings suggest that H2B S112 GlcNAcylation is a histone modification that facilitates H2BK120 monoubiquitination, presumably for transcriptional activation.

Some nuclear proteins have been shown to be GlcNAcylated by OGT, for example the enzymatic activity of histone H3K4 methyltransferase 5 (MLL5) is modulated by GlcNAcylation[7–9]. To identify chromatin substrates for OGT further, we screened for unknown GlcNAcylated glycoproteins in HeLa cell chromatin. GlcNAcylated proteins were purified by WGA lectin column chromatography and anti-GlcNAc antibody (clone RL2). Liquid chromatography–mass spectrometry (LC–MS)/MS analysis of the fraction revealed 284 factors, including previously reported GlcNAcylated glycoproteins[6,10] (Supplementary Table 1). Among the candidates, the enrichment of nucleosomes was confirmed by silver staining and western blotting (Supplementary Fig. 2), suggesting one or more histone(s) might have been GlcNAcylated. As OGT is the only known nuclear enzyme for protein GlcNAcylation[5], we asked whether histones served as substrates for OGT *in vitro* (Supplementary Fig. 3). H2A and H2B, as well as H2A variants (H2A.X and H2A.Z), but not H3 and H4, appeared to be GlcNAcylated (Fig. 1a). With histone octamers, H2B, but not H2A, appeared to serve as a substrate (Fig. 1b). Likewise, H2B in *Drosophila* histone was also GlcNAcylated (Supplementary Fig. 4), implying that H2B GlcNAcylation is conserved in metazoans.

A quadrupole (Q)-time of flight (TOF) MS assessment of the *in vitro* GlcNAcylated H2B showed that OGT could transfer three GlcNAc moieties to H2B (Supplementary Fig. 5). Electro-transfer-dissociation (ETD)–MS/MS mapped the sites to S91, S112 and S123 (Fig. 1c and Supplementary Fig. 6). Unlike a recent report[11], we were unable to detect the reported sites in H2B S36 and H4 S47. However, H2A T101 was detected as a GlcNAc site when H2A protein alone was used (data not shown). This discrepancy in identified GlcNAc sites might be due to differences in experimental approaches.

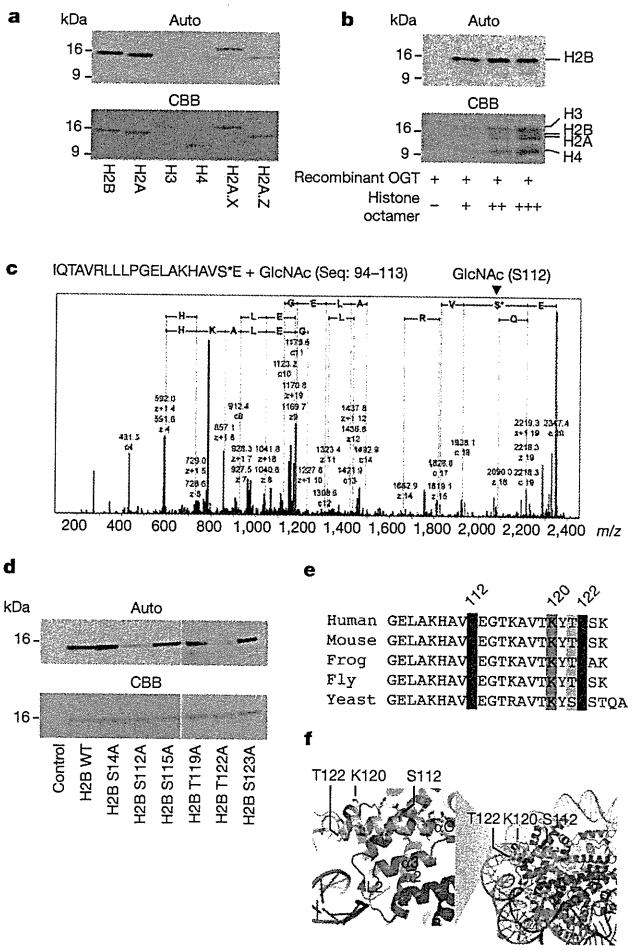

Figure 1 | H2B is GlcNAcylated at the C-terminal S112. a, b, *In vitro* OGT assay with recombinant histones (**a**) or the octamers reconstituted *in vitro* (**b**). Histones were GlcNAcylated by uridine diphosphate (UDP)-[^{3}H]GlcNAc and OGT, and the radiolabelled histones were subjected to autoradiography (top) and CBB staining (bottom). **c**, ETD–MS/MS scanned the GlcNAcylated peptides (2349.43 *m/z*) in Supplementary Fig. 5b. **d**, A series of H2B mutants at the indicated S/T was assessed by *in vitro* OGT assays. **e**, Sequence alignment of αC. **f**, The locations of the GlcNAc sites and the ubiquitination site of H2B in a nucleosome. The αC helix is illustrated as a white ribbon.

[1]Institute of Molecular and Cellular Biosciences, University of Tokyo, 1-1-1 Yayoi, Bunkyo-ku, Tokyo 113-0032, Japan. [2]Laboratory of Biochemistry and Molecular Biology, The Rockefeller University, New York, New York 10065, USA. [3]Department of Medical Oncology, Dana-Farber Cancer Institute and Harvard Medical School, Boston, Massachusetts 02115, USA. [4]Division of Cellular and Molecular Toxicology, National Institute of Health Sciences, 1-18-1 Kamiyoga, Setagaya-ku, Tokyo 158-8501, Japan. [5]ERATO, Japan Science and Technology Agency, Kawaguchi, Saitama 332-0012, Japan.

Next, *in vitro* OGT assays using peptide arrays covering full-length H2B revealed peaks at 101–115 peptides in the carboxy (C)-terminal α-helix (αC)[12] (Supplementary Fig. 7). This peptide was found to bear only one moiety by matrix-assisted laser desorption/ionization–time of flight (MALDI–TOF)/MS (Supplementary Fig. 8). Indeed, substitutions of S112 and T122 to A significantly reduced *in vitro* GlcNAcylation by OGT (Fig. 1d), but not mutations in the amino (N)-terminal tail (Supplementary Fig. 9). On the basis of these data, we concluded that the conserved S112 was a GlcNAc site in H2B, whereas T122 might be needed for recognition by OGT (Fig. 1e, f).

With our newly developed antibody (Supplementary Fig. 10), H2B S112 GlcNAc was detected in histones of HeLa cells. Depletion of glucose from the media for 24 h induced deglycosylation with neither overt cell death (Fig. 2a and Supplementary Fig. 11) nor alteration in histone acetylation marks of cell state indicators (H3 K14, H3 K56, H4 K16)[13,14] (Supplementary Fig. 12). H2B S112 GlcNAc could be restored by re-treatment with glucose at physiological concentrations (Supplementary Fig. 13).

Because many histone modifications are orchestrated, we tested if H2B S112 GlcNAc influenced H2B K120 monoubiquitination because of their proximity. After glucose depletion, replenishment of glucose gradually increased global GlcNAcylation of proteins, followed by H2B S112 GlcNAc and H2B monoubiquitination (Fig. 2b, c). Their reciprocal modifications disappeared when OGT was knocked down (Fig. 2d and Supplementary Fig. 14). In addition, in the immunoprecipitates of H2B containing the S112A and T122A double mutations (H2B AA), no response of K120 monoubiquitination to extracellular glucose was detected (Fig. 2e and Supplementary Fig. 15). Conversely, GlcNAcylation of H2B S112 was observed, even when K120 was mutated to R (Fig. 2e). From these findings, we conclude that H2B K120 monoubiquitination is mediated, at least in part, through S112 GlcNAcylation.

As glucosamine, but not pyruvate, potentiated H2B S112 GlcNAc (Fig. 2f), it appeared that this GlcNAcylation step was dependent on the HBP. To clarify this point, two HBP inhibitors (DON and AZA) were tested (Supplementary Information). After glucose depletion from media, these inhibitors attenuated the effect of glucose in H2B S112 GlcNAcylation along with K120 monoubiquitination (Fig. 2f).

In yeast, it was previously shown that H2B K120 monoubiquitination was induced by carbohydrates by glycolysis[15]. To address this issue, inhibitors of both glycolysis and deGlcNAcylation were applied to assess the crosstalk between the two modifications. When the cells were treated with iodoacetate, which blocks glycolysis but not HBP[15], the glucose effects on histone modifications were impaired, whereas the additional treatment of an OGA inhibitor (PUGNAc) restored both H2B S112 and K120 monoubiquitination (Supplementary Fig. 16). These data support the notion that H2B S112 GlcNAc senses decreases in glucose levels below normal levels and acts to promote H2B monoubiquitination, a modification that is associated with active transcription. Together with the fact that OGT is absent in yeast[6], the present H2B S112 GlcNAc-dependent pathway appears to constitute a system capable of sensing nutritional states in metazoans.

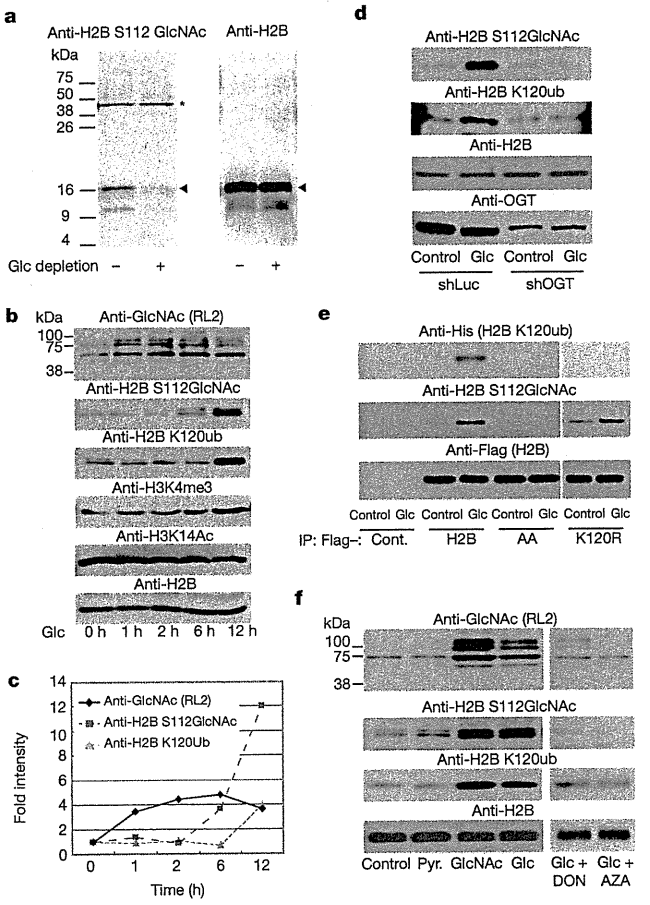

Figure 2 | H2B S112 GlcNAc is a glucose-responsive modification linked to K120 monoubiquitination (ub). **a**, Chromatin was prepared from HeLa cells cultured in media with or without 1 g l^{-1} glucose (Glc) for 24 h, and subjected to western blotting. Arrowheads show the indicated proteins. Asterisks indicate non-specific band. **b**, **c**, After 24 h Glc depletion, chromatin samples were prepared from HeLa cells treated with 4.5 g l^{-1} Glc for the indicated time. The intensities of the western blotting bands (**b**) were quantified (**c**). **d**, **e**, The effects of OGT knockdown (**d**) or H2B mutations (**e**) on H2B modifications after Glc replenishment. **f**, Western blotting analysis of the H2B modifications in HeLa cells that were cultured in DMEM without Glc (Cont.), or supplemented with 1 mM pyruvate (Pyr.), 10 mM GlcNAc or 4.5 g l^{-1} Glc with or without HBP inhibitors, 6-diazo-5-oxo-L-norleucine (100 μM, DON) or azaserine (100 μM, AZA).

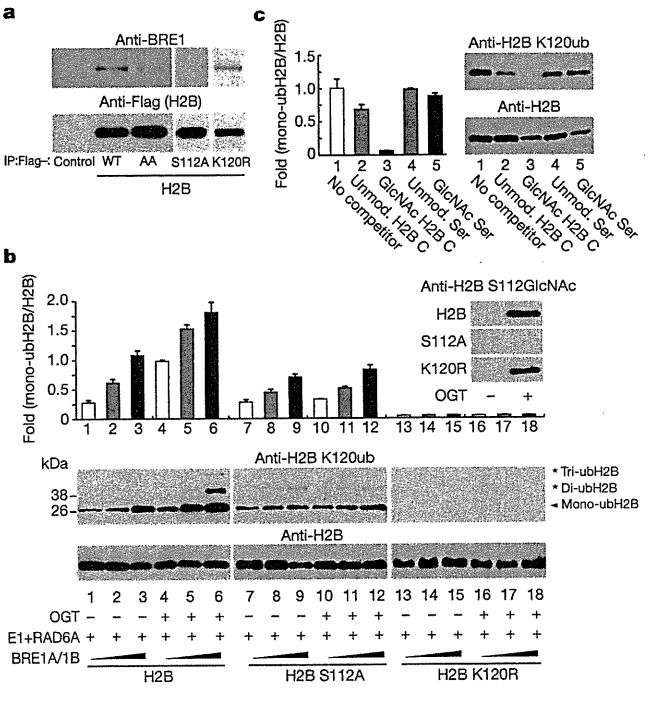

Figure 3 | GlcNAcylation at S112 facilitates ubiquitination at K120 in H2B. **a**, Western blotting analysis of the interaction of H2B mutants with BRE1A. **b**, **c**, *In vitro* monoubiquitination assay with GlcNAcylated H2B (**b**), or in the presence of competitor peptides (**c**). H2B was GlcNAcylated *in vitro* (**b**, top right), and the reactants were subsequently ubiquitinated by H2B monoubiquitination ligase. The reaction was performed with the indicated competitor peptides (0.25 μg ml^{-1}) (**c**). H2B K120 monoubiquitination was detected by western blotting (**b**, bottom; **c**, right) and quantified (**b**, top; **c**, left). Error bars, means and s.d. ($n = 3$).

The terminal GlcNAc of polysaccharides reportedly serves as a recognition moiety for E3 monoubiquitination ligase[16]. Therefore, we proposed that H2B S112 GlcNAc affected K120 monoubiquitination by the BRE1A/1B complex[17]. Flag-tagged H2B, but not AA or S112A, was co-immunoprecipitated with BRE1A (Fig. 3a). This association was observed in the presence of physiological levels of glucose in the media, and BRE1A was bound to H2B S112 GlcNAc (Supplementary Fig. 17). We then assessed how the GlcNAcylation of H2B influenced its *in vitro* ubiquitination by E1, RAD6A (E2) and the BRE1A/1B complex (E3). Although H2B K120 could be substantially ubiquitinated only by the ligases (Supplementary Fig. 18), GlcNAcylation of H2B promoted subsequent H2B ubiquitination, but not its S112A mutant (Fig. 3b). Likewise, ubiquitination was significantly attenuated by the presence of an H2B-S112-GlcNAcylated peptide, but not by either the unmodified control peptide or by GlcNAcylated serine (Fig. 3c). On the basis of these results, we conclude that the GlcNAc moiety at H2B S112 may anchor H2B monoubiquitination ligase.

To illustrate the role of H2B S112 GlcNAc in chromatin regulation, its location was visualized on fly polytene chromosomes. H2B S112 GlcNAc was detected widely in euchromatin, and, as anticipated, its signal disappeared in an OGT-disrupted fly, sxc^{1}/sxc^{78} (Supplementary Fig. 19). H2B S112 GlcNAc overlapped with H3K4 me2 more than with H3K9 me2 or H3K27 me3 (Fig. 4a). Similarly, in immunostained HeLa cells, H2B S112 GlcNAc sites appeared exclusively in 4′,6-diamidino-2-phenylindole (DAPI)-poor areas (Supplementary Fig. 20). Thus, H2B S112 GlcNAc probably accumulates in active chromatin rather than inactive chromatin.

To determine the precise loci of H2B S112 GlcNAc in HeLa cells, we performed chromatin immunoprecipitation (ChIP) and high-throughput sequencing (ChIP-seq). We confirmed ChIP quality by enrichments of H2B GlcNAc as well as H3K4 me2 and H2B K120 monoubiquitination, but neither H3K9 me2 nor H3K27 me3 (Supplementary Fig. 21). A total of 47,375 peaks were found widely distributed over the genome (Supplementary Fig. 22). However, H2B S112 GlcNAc peaked near transcription start sites (TSS), whereas the distribution decreased at transcription termination sites (TTS) (Fig. 4b), suggesting that it correlated with transcriptional regulation. To test this assumption, the activities of genes harbouring H2B S112 GlcNAc near TSS were estimated by microarray analysis (Supplementary Table 2). The average profiles near TSS significantly correlated with gene activity (Fig. 4c). Moreover, the expression levels of the 1,299 genes were reliably measured, and 1,021 genes showed high expression (Supplementary Fig. 23a and Supplementary Table 3b). Moreover, gene ontology analysis revealed that there was an association of the genes harbouring H2B S112 GlcNAc to cellular metabolic processes (Supplementary Fig. 23b and Supplementary Table 3c).

Next, we analysed the genome-wide overlap of H2B S112 GlcNAc with K120 monoubiquitination. A total of 44,158 peaks of H2B K120 monoubiquitination were detected, and their average profiles near TSS were similar to those profiles of H2B S112 GlcNAc (Supplementary

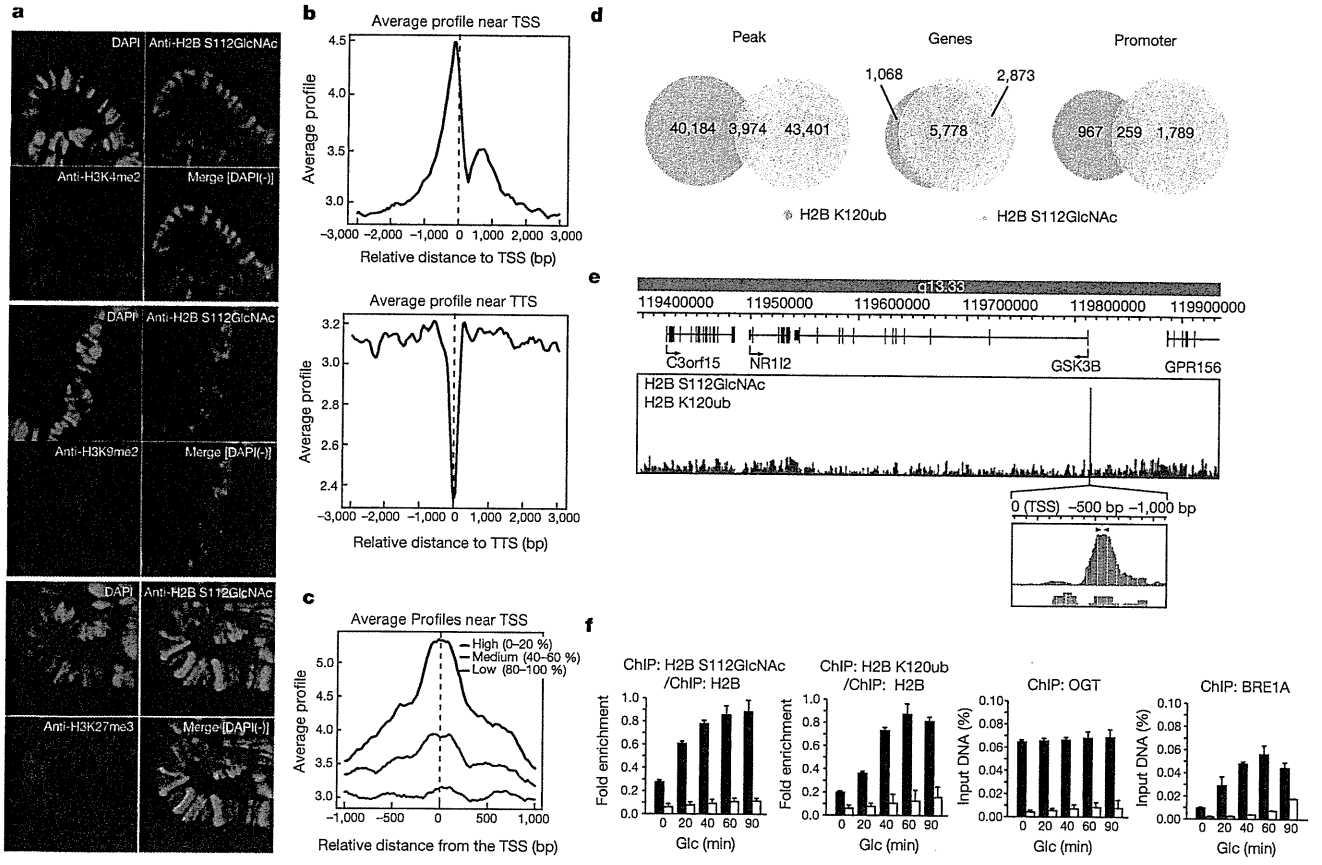

Figure 4 | GlcNAcylated H2B is associated with transcribed genes. **a**, Polytene staining with α-H2B S112 GlcNAc (green) and DAPI (blue) along with α-H3K4me2 (red, top), α-H3K9me2 (red, middle) or α-H3K27me3 (red, bottom). **b**–**e**, ChIP-seq analysis of the H2B S112 GlcNAc and K120 monoubiquitination. The distributions of H2B S112 GlcNAc were averaged near TSS (top) and TTS (bottom) (**b**). The average profiles of H2B S112 GlcNAc near TSS were calculated based on the associated gene activities (**c**). Venn diagrams showing overlap of the peaks (**d**, left), and the genes (**d**, middle) and the promoter (**d**, right) harbouring the modifications. The ChIP-seq profile surrounding the *GSK3B* gene (**e**). Arrowhead, position of qPCR primer. **f**, ChIP–qPCR validation in the GSK3B promoter. After Glc depletion, the control HeLa cells (black bar) and the OGT-knockdown cells (white bar) were replenished with Glc for 24 h. Then, the cells were subjected to ChIP with the indicated antibody and qPCR analysis. Error bars, means and s.d. ($n = 3$).

Fig. 24). Among the H2B K120 monoubiquitination peaks, nearly 10% (3,974 peaks) overlapped with H2B S112 GlcNAc peaks (Fig. 4d, left), and this evaluation was confirmed by a sequential ChIP–reChIP assay (Supplementary Fig. 25). Although 5,778 genes (66.8% of H2B S112 GlcNAc and 84.4% of K120 monoubiquitination) were found at the same loci (Fig. 4d, middle, and Supplementary Table 3d), 259 genes were identified when the two peaks were compared only within the promoters (Fig. 4d, right). The results of the ChIP-seq analysis were validated by ChIP–quantitative PCR (qPCR) assessment for the glycogen synthase kinase 3β (*GSK3B*) gene (Fig. 4e, f). These findings suggest that at several H2B S112 GlcNAc sites, it aids H2B monoubiquitination ligase recruitment whereas at others additional or different factors may be operational.

Here we provide evidence that histone GlcNAcylation is a post-translational modification correlated with active transcriptional events, and is responsive to serum glucose levels and/or cellular energy states in certain cell types (Supplementary Fig. 1). Using an antibody that specifically recognizes the S112 GlcNAc moiety of endogenous H2B, H2B was shown to serve as an OGT substrate. We have focused on the role of H2B S112 GlcNAcylation in gene regulation (Supplementary Fig. 1). Genome-wide analysis revealed that H2B S112 GlcNAc was frequently located near transcribed genes, suggesting that histone GlcNAcylation facilitates transcription of the genes. This idea is supported by previous reports that transcriptional output driven by several transcription factors is co-activated by OGT[9,18–20]. However, recent papers reported that *Drosophila* OGT is itself a polycomb group protein[8,21], and that many *O*-GlcNAcylated factors are involved in transcriptional repression and gene silencing[7,8]. In this respect, it will be interesting to identify other histone glycosylation sites and investigate their roles in transcriptional repression as well as activation.

METHODS SUMMARY

Plasmids and cell culture. All plasmids were generated with standard protocols (see Methods). Retrovirus production, infection and sorting of the infected cells followed previously reported protocols[9].

Purification of GlcNAc proteins from chromatin. Chromatin pellets were prepared from HeLa cells as previously described[22]. GlcNAc proteins were enriched with α-*O*-GlcNAc (RL2) antibody (Abcam) immobilized on Dynabeads (Invitrogen), and released with GlcNAc-*O*-serine.

Generation of monoclonal antibody. The synthetic H2B S112 GlcNAc peptide (CKHAV S(GlcNAc) EGTK) was used to immunize mice. The hybridomas were selected by enzyme-linked immunosorbent assay (ELISA) and western blotting analysis.

***In vitro* OGT and monoubiquitination assays.** Flag–OGT, Flag–E1, and Flag–BRE1A/BRE1B were purified by baculoviral systems, whereas histones and 6 × His-RAD6A were prepared from bacteria as previously reported[17,23]. H2B was incubated with OGT or H2B monoubiquitination ligases *in vitro*, and its modification was detected by western blotting as previously reported[9,23].

ChIP-seq and ChIP–qPCR. ChIP and ChIP-seq library construction was performed as previously described[24,25], and the libraries were sequenced to 50 base pairs (bp) with Hiseq2000 (Illumina). The fragments of interest in the libraries were quantified with specific promoter sets (Methods) by qPCR.

Full Methods and any associated references are available in the online version of the paper at www.nature.com/nature.

Received 16 July 2010; accepted 20 October 2011.
Published online 27 November 2011.

1. Strahl, B. D. & Allis, C. D. The language of covalent histone modifications. *Nature* **403,** 41–45 (2000).
2. Kouzarides, T. Chromatin modifications and their function. *Cell* **128,** 693–705 (2007).
3. Li, B., Carey, M. & Workman, J. L. The role of chromatin during transcription. *Cell* **128,** 707–719 (2007).
4. Berger, S. L. The complex language of chromatin regulation during transcription. *Nature* **447,** 407–412 (2007).
5. Hart, G. W., Housley, M. P. & Slawson, C. Cycling of O-linked β-*N*-acetylglucosamine on nucleocytoplasmic proteins. *Nature* **446,** 1017–1022 (2007).
6. Love, D. C. & Hanover, J. A. The hexosamine signaling pathway: deciphering the 'O-GlcNAc code'. *Sci. STKE* **2005,** re13 (2005).
7. Yang, X., Zhang, F. & Kudlow, J. E. Recruitment of O-GlcNAc transferase to promoters by corepressor mSin3A: coupling protein O-GlcNAcylation to transcriptional repression. *Cell* **110,** 69–80 (2002).
8. Gambetta, M. C., Oktaba, K. & Muller, J. Essential role of the glycosyltransferase sxc/Ogt in polycomb repression. *Science* **325,** 93–96 (2009).
9. Fujiki, R. *et al.* GlcNAcylation of a histone methyltransferase in retinoic-acid-induced granulopoiesis. *Nature* **459,** 455–459 (2009).
10. Wang, Z. *et al.* Extensive crosstalk between O-GlcNAcylation and phosphorylation regulates cytokinesis. *Sci. Signal.* **3,** ra2 (2010).
11. Sakabe, K., Wang, Z. & Hart, G. W. β-N-acetylglucosamine (O-GlcNAc) is part of the histone code. *Proc. Natl Acad. Sci. USA* **107,** 19915–19920 (2010).
12. Luger, K. *et al.* Crystal structure of the nucleosome core particle at 2.8 Å resolution. *Nature* **389,** 251–260 (1997).
13. Das, C., Lucia, M. S., Hansen, K. C. & Tyler, J. K. CBP/p300-mediated acetylation of histone H3 on lysine 56. *Nature* **459,** 113–117 (2009).
14. Dang, W. *et al.* Histone H4 lysine 16 acetylation regulates cellular lifespan. *Nature* **459,** 802–807 (2009).
15. Dong, L. & Xu, C. W. Carbohydrates induce mono-ubiquitination of H2B in yeast. *J. Biol. Chem.* **279,** 1577–1580 (2004).
16. Yoshida, Y. *et al.* E3 ubiquitin ligase that recognizes sugar chains. *Nature* **418,** 438–442 (2002).
17. Kim, J. *et al.* RAD6-Mediated transcription-coupled H2B ubiquitylation directly stimulates H3K4 methylation in human cells. *Cell* **137,** 459–471 (2009).
18. Dentin, R. *et al.* Hepatic glucose sensing via the CREB coactivator CRTC2. *Science* **319,** 1402–1405 (2008).
19. Chikanishi, T. *et al.* Glucose-induced expression of MIP-1 genes requires O-GlcNAc transferase in monocytes. *Biochem. Biophys. Res. Commun.* **394,** 865–870 (2010).
20. Jackson, S. P. & Tjian, R. O-glycosylation of eukaryotic transcription factors: implications for mechanisms of transcriptional regulation. *Cell* **55,** 125–133 (1988).
21. Sinclair, D. A. *et al. Drosophila* O-GlcNAc transferase (OGT) is encoded by the Polycomb group (PcG) gene, super sex combs (sxc). *Proc. Natl Acad. Sci. USA* **106,** 13427–13432 (2009).
22. Sawatsubashi, S. *et al.* A histone chaperone, DEK, transcriptionally coactivates a nuclear receptor. *Genes Dev.* **24,** 159–170 (2009).
23. Fujiki, R. *et al.* Ligand-induced transrepression by VDR through association of WSTF with acetylated histones. *EMBO J.* **24,** 3881–3894 (2005).
24. He, H. H. *et al.* Nucleosome dynamics define transcriptional enhancers. *Nature Genet.* **42,** 343–347 (2010).
25. Minsky, N. *et al.* Monoubiquitinated H2B is associated with the transcribed region of highly expressed genes in human cells. *Nature Cell Biol.* **10,** 483–488 (2008).

Supplementary Information is linked to the online version of the paper at www.nature.com/nature.

Acknowledgements We thank A. Miyajima, S. Saito and N. Moriyama for experimental support, and M. Yamaki for manuscript preparation. We also thank Y. Maekawa, J. Seta and N. Iwasaki for support with MS. This work was supported in part by The Naito Foundation, the Astellas foundation (to R.F.), the Ministry of Education, Culture, Sports, Science and Technology (MEXT) and the Japan Society for the Promotion of Science (to R.F. and S.K.).

Author Contributions S.K. planned the study with H.K.; R.G.R. and M.B. provided support and general guidance; R.F. designed the study and performed the experiments with H.S. (α-*O*-GlcNAc purification), A.Y. (LC–MS/MS), W.H. (*O*-GlcNAc site mapping), T.C. (*in vitro* OGT assay), S.I. (*Drosophila* analysis), Y.I., H.H.H. (ChIP-seq), F.O., J.K. (*in vitro* monoubiquitination assay), K.I. and J.K (microarray).

Author Information Reprints and permissions information is available at www.nature.com/reprints. The authors declare no competing financial interests. Readers are welcome to comment on the online version of this article at www.nature.com/nature. Correspondence and requests for materials should be addressed to S.K. (uskato@mail.ecc.u-tokyo.ac.jp).

METHODS

Plasmids and retroviruses. Complementary DNAs (cDNAs) of N-terminally Flag-tagged H2B and its mutant were subcloned into pcDNA3 (Invitrogen). A series of H2B point mutants were subcloned into the pET3 vector (Novagen). shRNA sequences targeting hOGT (5′-GCACATAGCAATCTGGCTTCC-3′) and *Renilla* luciferase (5′-TGCGTTGCTAGTACCAAC-3′, as a control) were inserted into the pSIREN-RetroQ-ZsGreen vector (Clontech). For retroviral production, the constructed shRNA vectors were transfected into PLAT-A cells. The virus contained in the medium was used for infection.

Generation of stable cell lines. To generate OGT-KD cells by retroviral infection, 10^6 cells were plated in 60 mm culture dishes, treated with 3 ml of retroviral cocktail (1 ml of the prepared retroviral solution plus 2 ml of DMEM with 10% FBS and 8 μg ml^{-1} polybrene), then cultured for another 48 h. A FACSVantage (BD) sorter was used to isolate the retrovirally transduced, enhanced green fluorescent protein (eGFP)-positive cells, as previously described[9]. To generate the cells stably expressing Flag-tagged constructs, HeLa cells were transfected with the pcDNA vectors encoding the Flag-tagged H2B or the AA mutant. The cells containing the integrated vectors were selected by exposure to 0.5 mg ml^{-1} G418.

Generation of monoclonal antibody. H2B S112 GlcNAc peptide (CKHAV S(GlcNAc) EGTK) was synthesized (MBL Institute) and used as an antigen (Operon Biotechnologies). The hybridomas were briefly screened using ELISA with the GlcNAc peptide, and finally selected by immunoblot analysis with the *in vitro* GlcNAcylated H2B.

Antibodies. Antibodies were obtained as follows: α-Flag M2 agarose (Sigma), α-H2A, α-H2B, α-H3, α-H4 (Abcam), α-H2B K120 monoubiquitination (Upstate), α-GlcNAc (RL2 or CTD110.6) (Abcam), α-OGT (Sigma), α-Flag (Sigma) and α-RNF20/BRE1A (Bethyl).

Purification and identification of GlcNAc proteins. The α-*O*-GlcNAc-immobilized beads were prepared with 15 μg α-*O*-GlcNAc (RL2) antibody and 0.5 ml of Dynabeads M-280 sheep α-mouse IgG (Invitrogen) according to the manufacturer's instructions. Chromatin extracts from HeLa cells (0.5 g protein) were prepared essentially as previously described[22]. In brief, the chromatin pellet, which consisted of residual material from the nuclear extract preparation with buffers supplemented with 1 mM streptozotocin (STZ), was re-suspended with micrococcal nuclease (MNase) buffer (20 mM Tris-HCl, 1 mM $CaCl_2$, 2 mM $MgCl_2$, 0.1 M KCl, 0.1% (v/v) Triton-X, 0.3 M sucrose, 1 mM DTT, 1 mM benzamidine, 0.2 mM PMSF, 1 mM STZ, pH 7.9). After addition of 3 U ml^{-1} MNase, the samples were incubated for 30 min at room temperature with continuous homogenization and the reaction was stopped by adding 5 mM EGTA and 5 mM EDTA. After centrifugation at 2,000*g* for 30 min at 4 °C, the supernatant (chromatin extract) was used for the following purification steps. The chromatin extracts were passed through a WGA agarose column (Vector). The flow-through fraction was further mixed with α-*O*-GlcNAc-immobilized beads and rotated for 8 h at 4 °C. After three washes with buffer D (20 mM Tris-HCl, 0.2 mM EDTA, 5 mM $MgCl_2$, 0.1 M KCl, 0.05% (v/v) NP-40, 10% (v/v) glycerol, 1 mM DTT, 1 mM benzamidine, 0.2 mM PMSF, 1 mM STZ, pH 7.9), glycoproteins were eluted twice with buffer D plus 0.4 mg ml^{-1} GlcNAc-*O*-serine (MBL) (elutions 1 and 2) and finally with 0.1 M glycine-HCl (pH2.0) (elution 3). Eluted proteins were desalted by methanol–chloroform precipitation, digested with trypsin (Promega) then loaded on the automated LC–MS/MS system, which was assembled with Zaplous nano-LC (AMR) plumbed with a reverse-phase C18 electrospray ionization (ESI) column (LC assist) and a Fiinigan LTQ ion-trap mass spectrometer (Thermo). The LC–MS/MS data were processed using Thermo BioWorks (Thermo) and SEQUEST (Thermo) for protein identification. The list of the identified proteins was further analysed by using the 'gene functional classification tool' in DAVID bioinformatics resources 6.7 (http://david.abcc.ncifcrf.gov/).

Recombinant proteins. Preparation of recombinant proteins was performed as previously reported[9,23]. Recombinant Flag–OGT, Flag–E1, Flag–BRE1A/B complexes were isolated by baculovirus expression and immunoprecipitation-based purification with α-Flag M2 agarose (Sigma). Recombinant 6 × His-RAD6A was expressed in bacteria and partly isolated with a HIS-Select Nickel Affinity Gel (Sigma). The eluate was diluted 1:20 with BC0 (20 mM HEPES, 0.2 mM EDTA, 10% (v/v) glycerol, pH 7.9), and fractionated with a Resource Q column (GE Healthcare) using a linear gradient (0–0.5 M KCl) method. Preparation of recombinant *Xenopus* histone H2B and its mutants was performed as previously described[9,23].

***In vitro* GlcNAcylation assay (autoradiographic analysis).** Recombinant Flag–OGT protein (0.5 μg) was incubated with 0.5 μg of recombinant histone and 0.2 mM (0.2 μCi) UDP-[^{3}H]GlcNAc (PerkinElmer) in a 25 μl reaction (50 mM Tris-HCl, 12.5 mM $MgCl_2$, 1 mM DTT, pH 7.5) for 24 h at 37 °C. The reaction was resolved with SDS–PAGE, blotted onto a polyvinylidene difluoride (PVDF) membrane, then subjected to autoradiography after spraying EN^{3}HANCE (NEN Lifescience).

***In vitro* GlcNAcylation assay (MS analysis).** Recombinant histones (1 μg) or recombinant histone octamers assembled *in vitro* (1 μg) were GlcNAcylated by recombinant Flag–OGT in 25 μl reactions (50 mM Tris-HCl, 2 mM UDP-GlcNAc, 12.5 mM $MgCl_2$, 1 mM DTT, pH 7.5) for 24 h at 37 °C. The reactions were directly subjected to a nano-LC ESI–TOF mass spectrometer system, which was assembled with a 1100 nanoLC (Agilent) plumbed with a ZORBAX 300SB-C18 column (Agilent) and micrOTOF (Bruker). Or, the reactions were digested with trypsin (Promega) and subjected to purification of glycopeptides with an MB-LAC WGA kit (Bruker). The enriched glycopeptides were loaded on the nano-LC ESI–ETD ion-trap mass-spectrometer system, which was assembled with the Agilent HP1200 Nano (Agilent) plumbed with ZORBAX 300SB-C18 (Agilent) and amaZon ETD (Bruker).

***In vitro* monoubiquitination assay.** GlcNAcylated histones (1 μg) were ubiquitinated with the E1 (0.1 μg), RAD6 (0.2 μg), BRE1 complex (0.5 μg), ubiquitin (3 μg) in 50 mM Tris (pH7.9), 5 mM $MgCl_2$, 4 mM ATP at 37 °C for 24 h.

ChIP-seq and ChIP-qPCR. ChIP and ChIP-seq libraries were constructed as previously described[24,25]. For ChIP-seq analysis, the libraries were sequenced to 50 bp with Hiseq2000 (Illumina). For ChIP–qPCR analysis, the fragments of interest in the libraries were quantified with Thermal Cycler TP800 (TAKARA) and SYBR Premix Ex Taq II (Takara). The qPCR primer sets for the *GSK3B* gene were 5′-TGCAAGCTCTCAGACGCTAA-3′ and 5′-CTCATTTCTCATGGGCG TTT-3′.

Biochemical and Biophysical Research Communications 412 (2011) 366–372

Contents lists available at ScienceDirect

Biochemical and Biophysical Research Communications

journal homepage: www.elsevier.com/locate/ybbrc

Genistein promotes DNA demethylation of the steroidogenic factor 1 (SF-1) promoter in endometrial stromal cells

Hiroshi Matsukura [a], Ken-ichi Aisaki [b], Katsuhide Igarashi [b], Yuko Matsushima [b], Jun Kanno [b], Masaaki Muramatsu [a], Katsuko Sudo [a,c], Noriko Sato [a,*]

[a] Department of Molecular Epidemiology, Medical Research Institute, Tokyo Medical and Dental University, 2-3-10 Kanda-surugadai, Chiyoda-ku, Tokyo 101-0062, Japan
[b] Division of Cellular and Molecular Toxicology, National Institute of Health Sciences, 1-18-1 Kamiyoga, Setagaya-ku, Tokyo 158-8501, Japan
[c] Animal Research Center, Tokyo Medical University, 6-1-1 Shinjuku, Shinjuku-ku, Tokyo 160-8402, Japan

ARTICLE INFO

Article history:
Received 21 July 2011
Available online 29 July 2011

Keywords:
Genistein
DNA methylation
Ovariectomized mice
Primary culture
Steroidogenic factor 1
High-resolution melting analysis

ABSTRACT

It has recently been demonstrated that genistein (GEN), a phytoestrogen in soy products, is an epigenetic modulator in various types of cells; but its effect on endometrium has not yet been determined. We investigated the effects of GEN on mouse uterine cells, *in vivo* and *in vitro*. Oral administration of GEN for 1 week induced mild proliferation of the endometrium in ovariectomized (OVX) mice, which was accompanied by the induction of steroidogenic factor 1 (SF-1) gene expression. GEN administration induced demethylation of multiple CpG sites in the SF-1 promoter; these sites are extensively methylated and thus silenced in normal endometrium. The GEN-mediated promoter demethylation occurred predominantly on the luminal side, as opposed to myometrium side, indicating that the epigenetic change was mainly shown in regenerated cells. Primary cultures of endometrial stromal cell colonies were screened for GEN-mediated alterations of DNA methylation by a high-resolution melting (HRM) method. One out of 20 colony-forming cell clones showed GEN-induced demethylation of SF-1. This clone exhibited a high proliferation capacity with continuous colony formation activity through multiple serial clonings. We propose that only a portion of endometrial cells are capable of receiving epigenetic modulation by GEN.

1. Introduction

Genistein (GEN), a major phytoestrogen in dietary soy, is a substantial component of the typical Asian and Western vegetarian diets, as well as recently developed infant soy milk formulas. There are several well known potential health benefits of GEN intake [1,2], one of which is an apparent decreased risk of breast and prostate cancers, based on human observational studies [1,3]. But GEN also paradoxically stimulates growth of breast cancer cells in culture [2] and uterine enlargement in rodents [4]. These effects may be mediated through estrogen receptor interactions and/or modulation of endogenous estrogen metabolism [5,6]. Since GEN can bind to estrogen receptors (ERs) α and β, with a stronger affinity to ERβ [5], it is categorized as a phyto-selective estrogen receptor modulator (SERM) [6,7]. The variations in GEN's agonistic or antagonistic effects may be affected by variations in endogenous estrogen levels. Previous studies have not determined whether the pleiotropic effects of GEN involve distinct epigenetic alteration. Recently, GEN was shown to alter DNA methylation in various types of cells, including ES cells [8], but most studies have been performed using cancer cell lines [9–11]. There have been few reports of the effects of GEN on DNA methylation in intact cells or *in vivo* [12]. In the present study, we utilized a uterotropic assay in ovariectomized (OVX) mice, as a model system to analyze epigenetic regulation by GEN.

In a previous study, high-dose GEN administration to OVX rats resulted in increased uterine weight and changed endometrial cell gene expression [6]. However, no epigenetic alterations were demonstrated under this condition. We selected the steroidogenic factor 1 (SF-1; official symbol: Nr5a1) gene as a target for the methylation analysis. SF-1 is an orphan nuclear receptor and transcription factor for key enzymes involved in steroidogenesis, such as StAR, Cyp11a1 (p450scc), Cyp17a1 (p450c17), and Cyp19a1 (aromatase) [13]. The SF-1 gene is not expressed in normal endometrium; however, SF-1 expression is reactivated in the disease state of human ectopic endometriosis, in which the SF-1 promoter is abnormally demethylated by an unknown mechanism [14]. The subsequent enhancement of steroidogenic genes and resultant local steroidogenesis are proposed to be important etiologies [15]. Therefore, we hypothesized that in mouse endometrial cells,

* Corresponding author. Fax: +81 3 5280 8058.
E-mail addresses: hmatsukura.epi@mri.tmd.ac.jp (Hiroshi Matsukura), nsato.epi@tmd.ac.jp (N. Sato).

0006-291X/$ - see front matter © 2011 Elsevier Inc. All rights reserved.
doi:10.1016/j.bbrc.2011.07.104

SF-1 might be subjected to epigenetic modulation by some external stimuli. Here we show that the SF-1 promoter was demethylated *in vivo* and *in vitro* by GEN treatment. This is the first demonstration of a phytoestrogen altering the epigenetic state of adult endometrium.

2. Materials and methods

2.1. Ethics statement

All procedures described here were performed according to protocols approved by the Animal Care Committee of the National Institute of Health Sciences, and Tokyo Medical and Dental University (No. 0110306A).

2.2. Oral administration of genistein to ovariectomized mice

C57BL/6JJmsSlc female mice (SLC) were used in this study. All mice were fed a phytoestrogen-free diet (Oriental Yeast) and were ovariectomized (OVX) 2 weeks prior to the genistein (GEN) treatment. OVX mice were divided into three different treatment groups, each consisting of 3–5 independent replicates, which orally received low-dose GEN (60 mg/kg/day), high-dose GEN (200 mg/kg/day), or vehicle (0.5% CMC-Na (Maruishi Pharmaceutical); 5 ml/kg/day) for 1 week. At the end of treatment (9 weeks of age), all mice were euthanized by exsanguination under ether anesthesia.

2.3. Uterotrophic assay and gene expression study after oral administration of genistein

Whole uteri were harvested, blotted, and weighted. Each uterus was divided into two horns, immediately placed into 2 ml plastic tubes of RNAlater solution (Ambion), and stored at 4 °C. From each sample, one horn was processed for mRNA expression analyses; RNAlater was replaced with 1.0 ml of RLT buffer (Qiagen), and the horn was homogenized by addition of a 5 mm diameter Zirconium bead (Funakoshi) and shaking with a MixerMill 300 (Qiagen) at 20 Hz for 5 min (only the outermost row of the shaker box was used). Further sample preparation and analysis were performed as previously described [16]. mRNA expressions were analyzed using Affymetrix Murine Genome 430 2.0 GeneChips, and calculated as copy number per cell by the Percellome method [16]. The second uterine horn of each sample was subjected to genomic DNA isolation.

2.4. Isolation of colony-forming cells derived from intact uteri

Five 8- to 9-week-old C57BL/6JJmsSlc female mice (SLC) were euthanized by cervical dislocation and whole uteri were harvested. Uterine horns were collected in Dulbecco's modified Eagle's medium/Hams F-12 (DMEM/F-12; Nacalai Tesque) containing 0.05 mg/ml gentamicin (Sigma–Aldrich). Each horn was dissected longitudinally and the endometrial tissue was divided into two portions: the luminal side and the myometrium side. A single cell suspension of endometrial cells was obtained using enzymatic digestion and mechanical means adapted from Chan et al. [17]. The tissue samples were minced and dissociated in 500 µl DMEM/F-12 containing 0.12 mg/ml (0.56 Wünsch U/ml) Blendzyme 2 and 40 µg/ml deoxyribonuclease type I (both from Roche Applied Science) in a shaking incubator (~90 rpm) at 37 °C. At 15 min intervals, the digests were pipetted to promote separation and cell dissociation was monitored microscopically. After 45 min, debris was filtered out using a 40-µm sieve (BD Biosciences). The single-cell suspensions were collected in DMEM/F-12 containing 10% FBS, 0.05 mg/ml gentamicin and stored on ice. Then the sieves were backwashed, and myometrial and glandular debris were further digested to single cells for 45 min as described above. All cell suspensions were filtered as described above, and combined. To remove erythrocytes, the cells were resuspended in 500 µl of HLB solution (Immuno Biological Laboratories) and incubated for 3 min. After washing twice with PBS, viable cell numbers were counted with trypan blue (Sigma–Aldrich). Cells were seeded on gelatin (0.1%, Sigma–Aldrich)-coated dishes at various densities of 0.1–3 × 10^5 cell/60-mm dish. After 14 days, non-overlapping clones were distinguished. Primary cell clones were expanded in DMEM/F-12 containing 5% FBS (SAFC Biosciences) and 0.05–0.1 mg/ml gentamicin, on gelatin-coated dishes.

2.5. Serial cloning of colony-forming cell clones

Self renewal was assessed by serial cloning of individual clones as described by Gargett et al. [18]. Cells were seeded on gelatin-coated 100-mm dishes at 10 cells/cm^2 (600 cells/100-mm dish). Culture medium was changed every 4 days and secondary clones formed distinct colonies by 14 days after plating. Secondary clones were similarly recloned to generate tertiary clones, and were also expanded in the same manner as the primary culture.

2.6. In vitro genistein exposure to colony-forming cells

From 70 isolated cell clones, we selected 20 clones from colonies that were composed of fibroblastic-shaped, homogenous cells with an average doubling time of less than 100 h. The selected clonal cells, whose passage number was less than 10, were subjected to *in vitro* GEN exposure. Cells were seeded on gelatin-coated 60-mm dishes, treated with or without 10 µM of GEN (dissolved in dimethylsulfoxide (DMSO)) in DMEM/F-12 containing 5% FBS and 0.05 mg/ml gentamicin for 7 days. The final DMSO concentration was 0.02%. The culture medium was changed every 2 days.

2.7. Genomic DNA preparation and bisulfite sequencing

Genomic DNA was isolated using a QIAamp DNA Mini Kit (QIAGEN) and 180 ng–1 µg was subjected to sodium bisulfite modification with a EpiTect Bisulfite Kit (QIAGEN) according to manufacturer's protocols. Bisulfite sequencing primers are shown in Supplementary Table 1. PCR products were cloned into the pT7 blue T vector (Novagen) and transformed into *Escherichia coli*. Plasmid DNA from positive colonies was purified and sequenced at the Tokyo Medical and Dental University Genome Laboratory (Tokyo, Japan). Sequence and statistical analyses were performed with the QUantification tool for Methylation Analysis; http://quma.cdb.riken.jp/top/quma_main_j.html [19]. The statistical significance of the difference between two bisulfite sequence groups at each CpG site was evaluated with Fisher's exact test.

2.8. Screening of DNA methylation status by high-resolution melting assay

All assays were performed on the LightCycler 480 using the LightCycler 480 High Resolution Melting Master kit, according to the manufacturer's instructions. Primers, designed using LightCycler Probe Design Software 2.0 (All, Roche Applied Science) are shown in Supplementary Table 1. All data were analyzed using LightCycler Gene Scanning Software.

2.9. Statistical analysis

Data are shown as means ± SD. Unpaired *t*-tests were used to compare the significance between two groups. Statistical analysis

was performed using Dr. SPSS 2 for Windows. Results were considered statistically significant at a P value of <0.05.

3. Results

3.1. Effects of genistein in uteri of ovariectomized (OVX) mice

OVX mice were fed with either vehicle (control) or low (60 mg/kg) or high (200 mg/kg) doses of GEN for 7 days and blotted uterus weights were determined (Fig. 1A). Compared to the control, low-dose GEN treatment did not significantly increase the uterus weight; high-dose treatment induced a slight but significant uterus enlargement (1.4-fold of control; $P < 0.005$). We then determined the mRNA expression levels of SF-1 (Fig. 1B) and steroidogenic genes (Fig. 1C–F) by the Percellome method. The mRNA levels of these genes were very low in the endometria from control and low-dose GEN-treatment groups, but were significantly increased (still less than one copy per cell on average) in the high-dose treatment group ($P < 0.05$), indicating that high-doses of GEN induced expression of these genes. Next, we determined the methylation status of SF-1 in

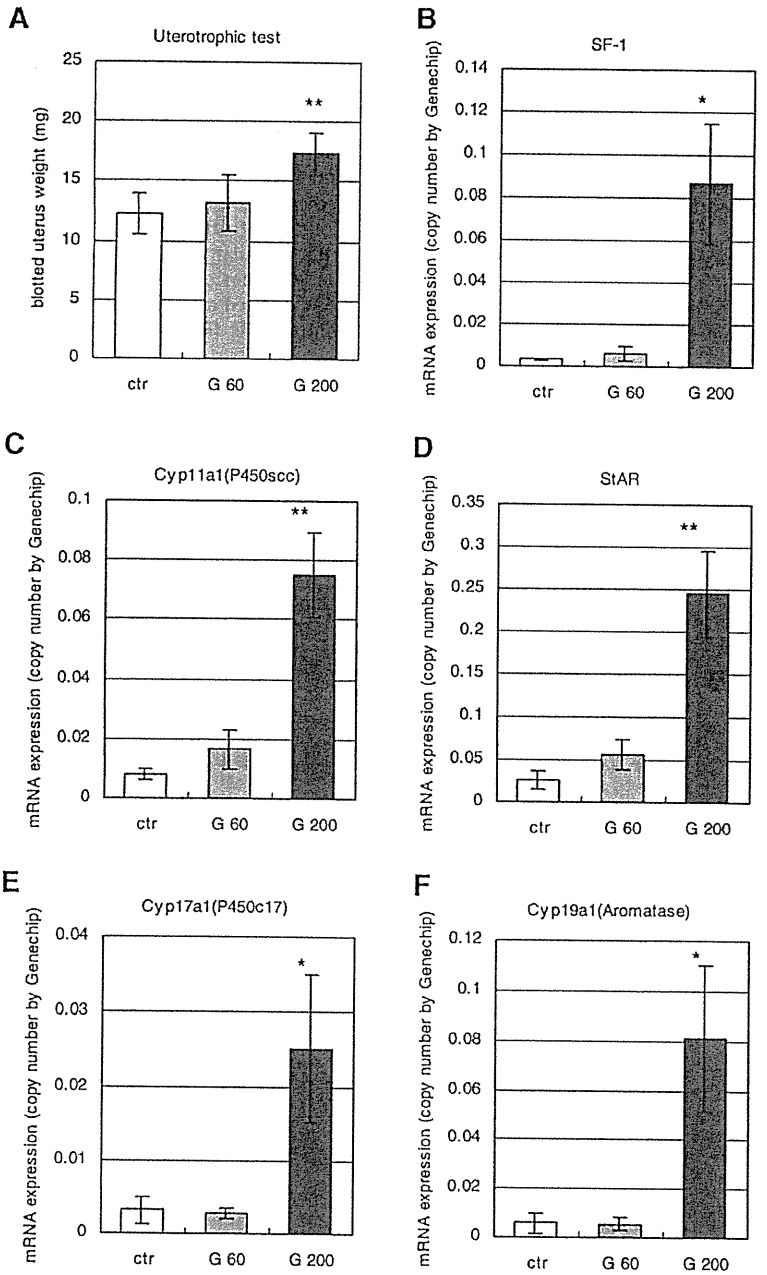

Fig. 1. Genistein induced endometrial regeneration and SF-1 mRNA expression in uterine tissue of OVX mice. (A) Blotted uterine weights were recorded. Control and GEN-treated groups comprised five and four mice, respectively. ctr; control, G 60; GEN 60 mg/kg/d, G200; GEN 200 mg/kg/d. (B–F) mRNA expressions of steroidogenic genes were determined using GeneChip analysis and were calculated by the Percellome method. Y axis indicates mRNA expression as copy number per cell. (B) SF-1 was determined by 1418315_at, (C) Cyp11a1 by 1439947_at, (D) StAR by 1418729_at, (E) Cyp17a1 by 1417017_at, and (F) Cyp19a1 by 1449920_at. *Statistically significant at $P < 0.05$. **Statistically significant at $P < 0.005$.

the total uterus tissues of the three groups of mice by bisulfite sequencing (Fig. 2A–C). There were 15 CpG sites spanning −272 to +199 of the promoter and the 5′-UTR (exon 1) region of SF-1. The percentages of total methylated CpG sites in this region, in control, and low and high-dose GEN, were 78.3%, 73.9%, and 54.4%, respectively, indicating that GEN dose-dependently induced demethylation in this region. Most CpG sites in the 5′-UTR (exon1) were demethylated by high-dose GEN. In particular, the methylation levels of 5 CpG sites between +45 and +89 were significantly lower in high-dose GEN than in control (Fisher's exact test, $P < 0.01$). We further split the endometrium to separate the luminal side (LU) from the basilar myometrial side (MY), and both specimens were separately subjected to bisulfite sequencing. This procedure was applied to the samples from the GEN-treated groups but not to control samples due to uterus atrophy. In low-dose GEN treated mice, the mean methylation levels of LU and MY were 84.8% and 65.0%, respectively (not shown). In high-dose GEN treated mice, the mean methylation levels of LU and MY were 42.1% and 66.7%, respectively (Fig. 2D). Thus, the demethylation induced by high-dose GEN occurred predominantly in the LU, rather than in the MY.

3.2. Effect of genistein on primary endometrial cell culture

In order to study the SF-1 promoter methylation at the cellular level, we employed an endometrial cell primary culture. Intact murine endometrium were divided into LU and MY portions, and cells were separately isolated. Primary cell clones were established by colony-formation, following the plating of a serially-titrated cell suspension (see Section 2). Efficient isolated colony formation was achieved with cells seeded at a density of 4,500–15,300 cells/cm^2. For LU and MY, the average frequencies of colony appearance were 7.5 per 10^5 cells and 15 per 10^5 cells, respectively. The growth curves of representative clones derived from LU and MY are shown in Fig. 3. Cell clones with highest and lowest proliferative activities were obtained from LU and MY, separately. More highly proliferative cells were obtained from MY than from LU (Fig. 3A and C). We selected 20 highly proliferative clones for further study (see Section 2). Two rapid growing clones obtained from MY showed self-renewal activity when secondarily seeded at a very low cell density (10 cells/cm^2) (not shown). To screen for primary cultured cells that responded to GEN, we set up a high-resolution melting (HRM) assay that identified region-specific methylation levels. The region analyzed by HRM assay exclusively contained the 7 CpG sites between +19 and +89 bp that were most differentially demethylated following oral administration of GEN (Fig. 2). Each clone was treated with or without GEN for 1 week; cells treated with a similar concentration of DMSO served as control. Among the 20 clones that we screened, only one GEN-treated clone (No. 16) exhibited a significant shift in the melting curve compared to control cells (Fig. 4A). This clone had the highest proliferation

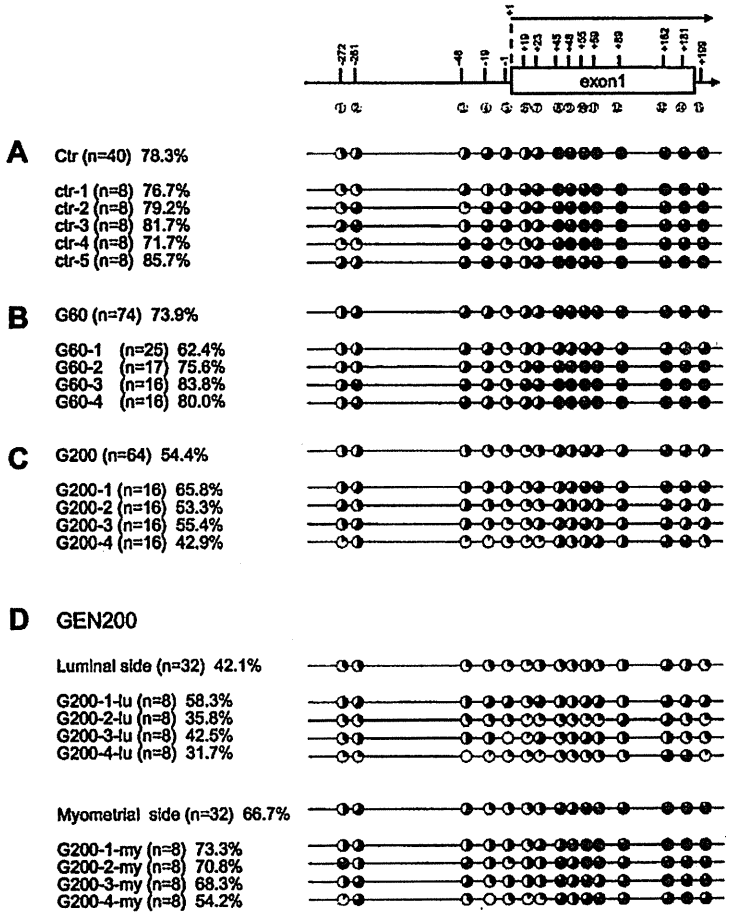

Fig. 2. Genistein induced demethylation of the SF-1 gene promoter in endometrial tissues of OVX mice. The schematic diagram indicates CpG locations on the SF-1 promoter region, spanning 5′-flanking to exon 1. The CpG position relative to the first base of exon 1 (+1) is shown. The bisulfite sequencing fragment contains 15 CpG sites. The black inlay represents the mean methylation levels of each CpG, and the left panel contains the number of sequenced clones and the mean methylation level of all CpGs. Summarized methylation results are shown at the top. (A–C) Difference in methylation levels between (A) vehicle (control), (B) low-dose GEN (60 mg/kg/d), and (C) high-dose GEN (200 mg/kg/d) exposed uteri. (D) Difference in methylation levels between luminal and myometrial sides of a uterus exposed to high-dose GEN.

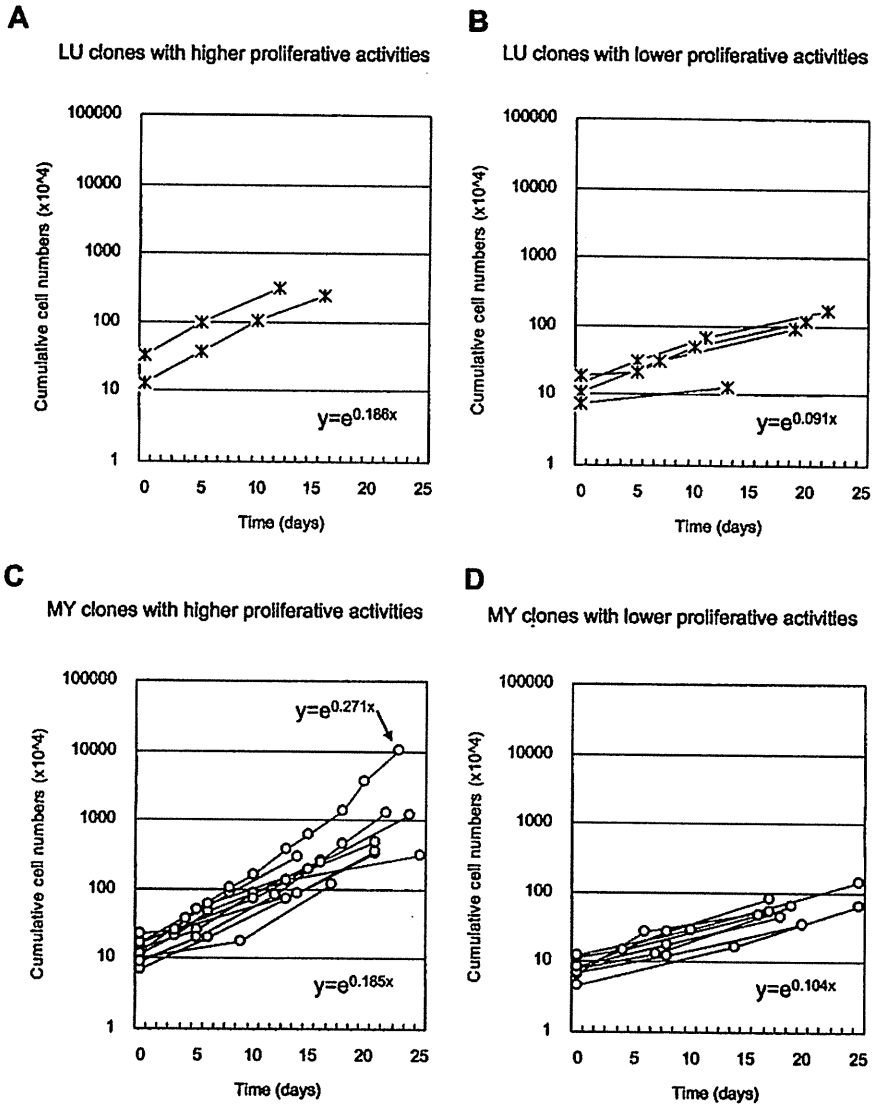

Fig. 3. Proliferation properties of isolated clones: one clone showed highly proliferative activity. Representative growth curves of clones harvested from intact murine endometrium are shown. Formula indicates the slope of fitted growth curves. Clones were divided into two groups: high and low proliferative (see Section 2). A total of 20 highly proliferative clones were analyzed by HRM after *in vitro* GEN treatment. (A, B) Asterisks indicate representative growth curves of cell clones isolated from luminal side. (A) Clones with higher proliferative activities, derived from luminal side. Six highly proliferative clones were obtained in total; 2 representatives are shown. (B) Clones with lower proliferative activities, derived from luminal side. (C, D) Each circle indicates representative growth curves of cell clones isolated from myometrial side. (C) Clones with higher proliferative activities, derived from the myometrial side. In total, 14 highly proliferative clones were obtained; 10 representatives are shown. The arrow indicates the clone with the most rapid growth. (D) Clones with lower proliferative activities, derived from myometrial side.

activity (Fig. 3C, arrow). GEN treatment of the other clones did not result in significant changes to the melting curve patterns (not shown). We further confirmed the methylation status of clone No. 16 by bisulfite sequencing. The percentages of CpG methylation in the SF-1-272 to +199 promoter regions for untreated and GEN-treated cells were 85.0% and 65.8%, respectively (Fig. 4B).

4. Discussion

Growing evidence suggests that the manner in which nutrients can either help maintain health, or conversely, promote disease development may be mediated by epigenetic regulation [12,20]. However, relatively little is known about tissue-specific sensitivity or how much plasticity exists in regards to the effect that a given environmental factor can exert on a certain epigenetic target [20,21]. GEN, a non-nutrient dietary component of soy products, exhibits mixed estrogen agonist and antagonist properties, and multiple functions both *in vivo* and *in vitro* [7,22]. Several animal studies have demonstrated that GEN acts as an epigenetic modulator [20]. We focused on the effects of GEN on endometrium, because endometrium is not only hormone responsive, but also a highly proliferative organ. Epigenetic alterations of proliferative tissue or cells may then be expanded through tissue proliferation. We used OVX rodents, which are a widely used model for studying estrogen withdrawal and replacement [23], as well as for the assessment of endocrine-disrupting chemicals in the environment [4]. In our experiment, GEN induced proliferation of the endometrium and increased uterine weight (Fig. 1A) to extents similar to those previously reported in OVX rats [4]. Our findings also suggested that GEN treatment induced marked demethylation of

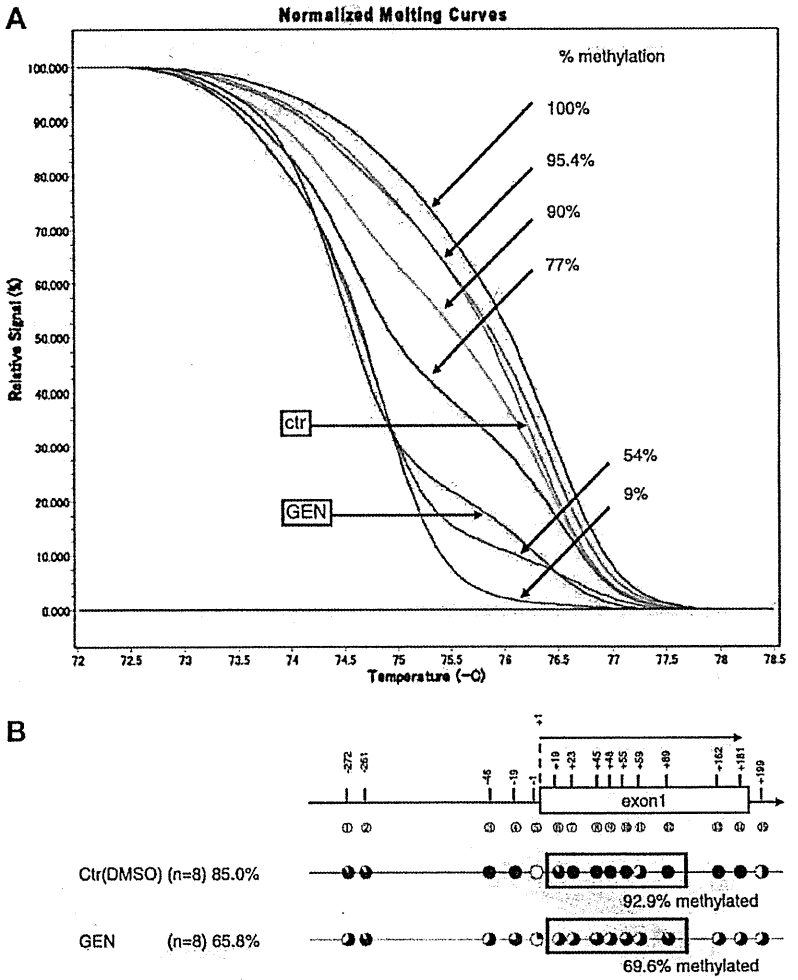

Fig. 4. Genistein induced demethylation of the SF-1 gene in the cell clone that showed the highest proliferative activity. (A) The GEN-mediated demethylation of CpGs (at the positions of +19, 23, 45, 48, 55, 59, and 89) in the SF-1 gene *in vitro* in one out of 20 isolated clones (Fig. 3A and C). HRM analysis enabled to clear separation of the PCR product mixtures with different CpG compositions. The methylation standards were prepared as 100% (red), 95.4% (orange), 90% (yellow), 77% (green), 54% (blue), and 9% (violet) methylated template in demethylated background. Grey and pink indicate the control and GEN-treated clone sample, respectively. (B) SF-1 DNA methylation status, obtained from bisulfate sequencing, of the clone that showed demethylation in HRM assay. Percentage under box (HRM region) indicates percent methylation of HRM region. (For interpretation of the references to color in this figure legend, the reader is referred to the web version of this paper.)

CpG sites in the SF-1 promoter (Fig. 2), and substantial increase in SF-1 mRNA level (Fig. 1B). Expressions of genes downstream of transcription factor SF-1 were also significantly enhanced (Fig. 1C–F). However, it should be noted that the induced mRNA levels were still very low (Fig. 1B–F), less than one copy per cell, as determined by the Percellome method [16]. Our results are consistent with those of a previous study reporting that a physiological concentration of GEN increased Cyp19a1 enzymatic activity in endometrial cells derived from a normal uterus, whereas GEN did not affect Cyp19a1 activity in a cell-free assay [24]. It is unknown whether GEN stimulated Cyp19a1 activity by epigenetic modulation.

In the present study, we also identified primary cultured endometrial cells that were competent for epigenetic regulation by GEN, which were present at a very low frequency. In our *in vitro* study, GEN treatment did not enhance, but rather inhibited the proliferation of colony-derived cells. Taken together, these findings indicate that a minor population of endometrium cells can respond to GEN and that, in these cells, GEN induces demethylation and activation of SF-1, followed by the induction of the SF-1 steroidogenic cascade. This might lead to local steroidogenesis and enhanced endometrium proliferation *in vivo* in GEN-treated OVX mice. Since demethylation of the SF-1 promoter was observed at the whole tissue level (Fig. 2), and the induced expression of steroidogenic genes occurred only to a subcellular amount (Fig. 1B–F), the demethylation event in each cell may not be sufficient for the SF-1 induction.

The demethylation in the endometrium that occurred after 1 week of treatment with high-dose GEN was more prominent in the LU than in the MY. Following GEN treatment, the methylation level in the MY was similar to that in the untreated endometrium as a whole. After 7 days of GEN exposure, the endometrial cells in the LU of OVX mice were composed of regenerated cells moving from MY to LU; in light of this, our results indicate that the initial epigenetic alteration might be expanded through proliferation of regenerating cells. This is also consistent with our observation that more endometrial cells derived from MY showed higher colony-formation activity and rapid proliferation than did those derived

from LU (Fig. 3). We thus speculate that there are GEN-sensitive cells in the MY, which might contain endometrial stem cells [25].

Recently, human endometrial stem cells were identified; they reside in endometrial stromal tissue and possess fibroblastic-shape and self-renewal ability, thus forming large, densely packed, homogenous colonies [17,18]. Some candidates for murine endometrial progenitor cells have been suggested to reside in the luminal epithelial or area of adjacent to the myometrium [25]. The rapidly growing endometrial cell that we obtained had a fibroblastic-shape, formed large, relatively homogenous, densely packed colonies, and showed self-renewal activity when seeded at a very low cell density (data not shown). Although there are differences between the species, we speculate that our rapid growing cell clones may correspond to the human endometrial stromal progenitors cells [17].

Aberrant SF-1 expression with lack of promoter CpG methylation has been reported in ectopic endometriosis [14], and thus endometriosis is now considered an epigenetic disease [26]. Endometriosis is classically defined as the growth of endometrial tissue at extrauterine sites; it has been suggested that each endometriotic lesion originates from a single epigenetically deregulated endometrial progenitor cell [27]. Further studies are required to identify cells which are competent for epigenetic changes following GEN exposure, and to elucidate the relationships between these cells, GEN, and endometriosis.

In conclusion, we demonstrated that GEN demethylates the promoter region of the SF-1 gene. This is the first demonstration of phytoestrogen participation in epigenetic alterations in adult endometrial tissue. These findings are important from standpoints of nutrition, public health, and disease prevention. Further study is warranted to characterize the nature of the cells that respond to GEN in the endometrium.

Appendix A. Supplementary data

Supplementary data associated with this article can be found, in the online version, at doi:10.1016/j.bbrc.2011.07.104.

References

[1] H. Adlercreutz, Phyto-oestrogens and cancer, Lancet Oncol. 3 (2002) 364–373.
[2] M. Messina, W. McCaskill-Stevens, J.W. Lampe, Addressing the soy and breast cancer relationship: review, commentary, and workshop proceedings, J. Natl. Cancer Inst. 98 (2006) 1275–1284.
[3] A.H. Wu, R.G. Ziegler, A.M. Nomura, D.W. West, L.N. Kolonel, P.L. Horn-Ross, R.N. Hoover, M.C. Pike, Soy intake and risk of breast cancer in Asians and Asian Americans, Am. J. Clin. Nutr. 68 (1998) 1437S–1443S.
[4] J. Kanno, L. Onyon, S. Peddada, J. Ashby, E. Jacob, W. Owens, The OECD program to validate the rat uterotrophic bioassay. Phase 2: dose–response studies, Environ. Health Perspect. 111 (2003) 1530–1549.
[5] K. Pettersson, J.A. Gustafsson, Role of estrogen receptor beta in estrogen action, Annu. Rev. Physiol. 63 (2001) 165–192.
[6] P. Diel, T. Hertrampf, J. Seibel, U. Laudenbach-Leschowsky, S. Kolba, G. Vollmer, Combinatorial effects of the phytoestrogen genistein and of estradiol in uterus and liver of female Wistar rats, J. Steroid Biochem. Mol. Biol. 102 (2006) 60–70.
[7] V. Beck, U. Rohr, A. Jungbauer, Phytoestrogens derived from red clover: an alternative to estrogen replacement therapy?, J Steroid Biochem. Mol. Biol. 94 (2005) 499–518.
[8] N. Sato, N. Yamakawa, M. Masuda, K. Sudo, I. Hatada, M. Muramatsu, Genome-wide DNA methylation analysis reveals phytoestrogen modification of promoter methylation patterns during embryonic stem cell differentiation, PLoS One 6 (2011) e19278.
[9] S.M. Meeran, A. Ahmed, T.O. Tollefsbol, Epigenetic targets of bioactive dietary components for cancer prevention and therapy, Clin. Epigenetics 1 (2010) 101–116.
[10] S. Majid, A.A. Dar, V. Shahryari, H. Hirata, A. Ahmad, S. Saini, Y. Tanaka, A.V. Dahiya, R. Dahiya, Genistein reverses hypermethylation and induces active histone modifications in tumor suppressor gene B-Cell translocation gene 3 in prostate cancer, Cancer 116 (2010) 66–76.
[11] A.K. Jha, M. Nikbakht, G. Parashar, A. Shrivastava, N. Capalash, J. Kaur, Reversal of hypermethylation and reactivation of the RARbeta2 gene by natural compounds in cervical cancer cell lines, Folia. Biol. (Praha) 56 (2010) 195–200.
[12] Y. Li, T.O. Tollefsbol, Impact on DNA methylation in cancer prevention and therapy by bioactive dietary components, Curr. Med. Chem. 17 (2010) 2141–2151.
[13] K. Morohashi, S. Honda, Y. Inomata, H. Handa, T. Omura, A common trans-acting factor, Ad4-binding protein, to the promoters of steroidogenic P-450s, J. Biol. Chem. 267 (1992) 17913–17919.
[14] Q. Xue, Z. Lin, P. Yin, M.P. Milad, Y.H. Cheng, E. Confino, S. Reierstad, S.E. Bulun, Transcriptional activation of steroidogenic factor-1 by hypomethylation of the 5′ CpG island in endometriosis, J. Clin. Endocrinol. Metab. 92 (2007) 3261–3267.
[15] S.E. Bulun, H. Utsunomiya, Z. Lin, P. Yin, Y.H. Cheng, M.E. Pavone, H. Tokunaga, E. Trukhacheva, E. Attar, B. Gurates, M.P. Milad, E. Confino, E. Su, S. Reierstad, Q. Xue, Steroidogenic factor-1 and endometriosis, Mol. Cell. Endocrinol. 300 (2009) 104–108.
[16] J. Kanno, K. Aisaki, K. Igarashi, N. Nakatsu, A. Ono, Y. Kodama, T. Nagao, "Per cell" normalization method for mRNA measurement by quantitative PCR and microarrays, BMC Genomics 7 (2006) 64.
[17] R.W. Chan, K.E. Schwab, C.E. Gargett, Clonogenicity of human endometrial epithelial and stromal cells, Biol. Reprod. 70 (2004) 1738–1750.
[18] C.E. Gargett, K.E. Schwab, R.M. Zillwood, H.P. Nguyen, D. Wu, Isolation and culture of epithelial progenitors and mesenchymal stem cells from human endometrium, Biol. Reprod. 80 (2009) 1136–1145.
[19] Y. Kumaki, M. Oda, M. Okano, QUMA: quantification tool for methylation analysis, Nucleic Acids Res. 36 (2008) W170–W175.
[20] J.A. McKay, J.C. Mathers, Diet induced epigenetic changes and their implications for health, Acta Physiol. (Oxf) (2011) 103–118.
[21] B.C. Christensen, E.A. Houseman, C.J. Marsit, S. Zheng, M.R. Wrensch, J.L. Wiemels, H.H. Nelson, M.R. Karagas, J.F. Padbury, R. Bueno, D.J. Sugarbaker, R.F. Yeh, J.K. Wiencke, K.T. Kelsey, Aging and environmental exposures alter tissue-specific DNA methylation dependent upon CpG island context, PLoS Genet. 5 (2009) e1000602.
[22] C.B. Klein, A.A. King, Genistein genotoxicity: critical considerations of in vitro exposure dose, Toxicol. Appl. Pharmacol. 224 (2007) 1–11.
[23] G. Rimoldi, J. Christoffel, D. Seidlova-Wuttke, H. Jarry, W. Wuttke, Effects of chronic genistein treatment in mammary gland, uterus, and vagina, Environ. Health Perspect. 115 (Suppl. 1) (2007) 62–68.
[24] K.M. Edmunds, A.C. Holloway, D.J. Crankshaw, S.K. Agarwal, W.G. Foster, The effects of dietary phytoestrogens on aromatase activity in human endometrial stromal cells, Reprod. Nutr. Dev. 45 (2005) 709–720.
[25] C.E. Gargett, H. Masuda, Adult stem cells in the endometrium, Mol. Hum. Reprod. 16 (2010) 818–834.
[26] S.W. Guo, Epigenetics of endometriosis, Mol. Hum. Reprod. 15 (2009) 587–607.
[27] Y. Wu, Z. Basir, A. Kajdacsy-Balla, E. Strawn, V. Macias, K. Montgomery, S.W. Guo, Resolution of clonal origins for endometriotic lesions using laser capture microdissection and the human androgen receptor (HUMARA) assay, Fertil. Steril. 79 (Suppl. 1) (2003) 710–717.

NANOS2 interacts with the CCR4-NOT deadenylation complex and leads to suppression of specific RNAs

Atsushi Suzuki[a], Katsuhide Igarashi[b], Ken-ichi Aisaki[b], Jun Kanno[b], and Yumiko Saga[c,1]

[a]Interdisciplinary Research Center, Yokohama National University, Yokohama, Kanagawa 240-8501, Japan; [b]Cellular and Molecular Toxicology Division, National Institute of Health Sciences, Setagayaku, Tokyo 158-8501, Japan; and [c]Division of Mammalian Development, National Institute of Genetics, Mishima 411-8540, Japan

Edited by Ruth Lehmann, New York University Medical Center, New York, NY, and approved December 30, 2009 (received for review August 2, 2009)

Nanos is one of the evolutionarily conserved proteins implicated in germ cell development. We have previously shown that NANOS2 plays an important role in both the maintenance and sexual development of germ cells. However, the molecular mechanisms underlying these events have remained elusive. In our present study, we found that NANOS2 localizes to the P-bodies, known centers of RNA degradation that are abundantly accumulated in male gonocytes. We further identified by immunoprecipitation that the components of the CCR4-NOT deadenylation complex are NANOS2-interacting proteins and found that NANOS2 promotes the localization of CNOT proteins to P-bodies in vivo. We also elucidated that the NANOS2/CCR4-NOT complex has deadenylase activity in vitro, and that some of the RNAs implicated in meiosis interact with NANOS2 and are accumulated in its absence. Our current data thus indicate that the expression of these RNA molecules is normally suppressed via a NANOS2-mediated mechanism. We propose from our current findings that NANOS2-interacting RNAs may be recruited to P-bodies and degraded by the enzymes contained therein through NANOS2-mediated deadenylation.

germ cells | P-body | meiosis

In the mouse, the primordial germ cells (PGCs) are segregated from the somatic cell lineage at an early gastrulation stage (1). Although the PGCs are potent producers of both oogonia and spermatogonia, sexual differentiation is induced after their colonization of the embryonic gonads with somatic cells. However, the initial steps leading to diversification of these cells have long remained unsolved. Retinoic acid (RA) signaling has recently been identified as the initial trigger for feminization (2). RA molecules derived from the mesonephros trigger meiotic initiation in female gonocytes via the induction of the RA responsive gene *Stra8*, which is required for premeiotic replication (3). In contrast, male gonocytes are protected from exposure to RA by CYP26B1, an RA metabolizing enzyme produced from somatic cells, resulting in the suppression of meiosis up to E13.5 (4, 5). In addition, *Nanos2* expression begins after E13.5 and is required for the maintenance and promotion of the male germ cell state (6).

Nanos is an evolutionarily conserved RNA-binding protein that is essential for germ cell development (7). In *Drosophila*, Nanos forms a complex with another RNA-binding protein, Pumilio, and represses the translation of the *hunchback*, *cyclin B*, and *hid* mRNAs thereby establishing embryonic polarity, mitotic quiescence, and suppression of apoptosis, respectively (8–10). Three *Nanos* homologs, *Nanos1–3*, exist in the mouse, among which *Nanos3* and *Nanos2* are expressed in the germ cells and are required to protect these cells from undergoing apoptosis during migration and after colonization of the male gonads, respectively (11, 12). In addition, *Nanos2* plays a key role during the sexual development of germ cells by suppressing meiosis and promoting male-type differentiation in the embryonic male gonads. Moreover, the forced expression of *Nanos2* in female gonocytes can induce the suppression of meiosis and promotion of male-type gene expression (6). However, the molecular mechanisms underlying how this protein accomplishes such pleiotropic functions in the mouse germ cells remain unknown.

In our present study, we find that NANOS2 localizes to P-bodies, a central hub of RNA degradation (13, 14). We further identify components of the CCR4-NOT deadenylation complex as NANOS2-associated proteins in vivo, which can cleave poly(A) RNA in vitro. We also show that specific mRNAs interact with NANOS2, and thus propose that NANOS2 plays a role in recruiting the CCR4-NOT deadenylation complex to trigger the degradation of specific RNAs.

Results

NANOS2 Localizes at P-Bodies During Gonocyte Development. To increase our understanding of the molecular mechanisms underlying the function of the NANOS2 protein, we first analyzed the cellular localization of this protein by immunostaining. Consistent with the results of our previous western analyses (15), NANOS2 protein was first detectable at E13.5 in the cytoplasm of male mouse gonocytes. This signal intensity increased until about E16.5 and then slightly decreased by E17.5. In addition, we found that some of the NANOS2 proteins formed discrete foci, the number of which gradually increased until E16.5 and then decreased thereafter (Fig. S1 *A–F*). Because *Drosophila* Vasa and Tudor are known to form cytoplasmic foci (16, 17), which are the polar granules in the germ plasm, we speculated that these NANOS2 foci might colocalize with the mouse homologs of Vasa, MVH (mouse vasa homolog) (18) and the Tudor protein TDRD1 (tudor domain containing 1) (19). However, these foci did not show any clear colocalization with NANOS2 (Fig. S2 *A–F*). We next tested the possibility that the NANOS2 foci might correspond to P-bodies, which are known to function as a center of RNA degradation. We thus conducted double-immunostaining using antibodies against the P-body components DCP2 and XRN1, an mRNA decapping enzyme and RNA exonuclease, respectively (13, 14). We were initially surprised to find that many P-bodies could be specifically observed only in germ cells and not in the somatic cells in E15.5 male gonads, and also that the NANOS2 foci clearly merged with those of DCP2 and XRN1 (Fig. 1 *A–F*) from E13.5 to E17.5 (Fig. S3 *A–F*). This suggests the possibility that NANOS2 may be involved in RNA degradation.

Nanos2 Functions in the Formation of P-Bodies. We further examined the status of the P-bodies in the mouse gonads of both sexes by immunostaining of p54/RCK, a homolog of *Drosophila* Me31B and also a marker of these structures (20). Although the P-bodies seemed to be present in the same number and size in the gonocytes of both sexes at E12.5, they were gradually reduced and eventually lost by E14.5 in female gonocytes (Fig. S4 *E* and *F*). In contrast, the P-bodies become much larger in both number and

Author contributions: A.S. and Y.S. designed research; A.S., performed research; K.I., K.. A., and J.K. analyzed data of microarray analyses; and A.S. and Y.S. wrote the paper.

The authors declare no conflict of interest.

This article is a PNAS Direct Submission.

[1]To whom correspondence should be addressed. E-mail: ysaga@lab.nig.ac.jp.

This article contains supporting information online at www.pnas.org/cgi/content/full/0908664107/DCSupplemental.

www.pnas.org/cgi/doi/10.1073/pnas.0908664107

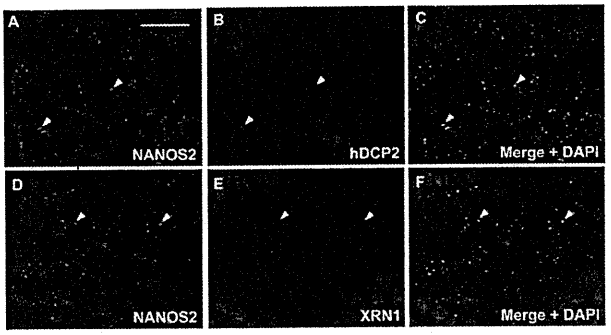

Fig. 1. NANOS2 localizes to the P-bodies in male mouse gonocytes. (*A–L*) Sections prepared from wild-type E15.5 male gonads were double-stained with mouse anti-NANOS2 (green) (*A* and *D*) and either hDCP2 (*B*) or mXRN1 (*E*) antibodies (red staining in each case). Arrowheads indicate colocalization of NANOS2 and hDCP2 (*C*) or XRN1 (*F*). DNA was counterstained with DAPI (blue). (Scale bar in *A*, 20 μm for all panels.)

size from E14.5, concomitant with the onset of NANOS2 expression, in male gonocytes (Fig. S4 *A–D*).

To further explore the role of NANOS2 in P-body formation, we examined the status of these structures in the absence of *Nanos2*. Although there were, somewhat unexpectedly, many P-bodies detected in both *Nanos2*$^{+/-}$ and *Nanos2*$^{-/-}$ male gonocytes at E13.5, their sizes became gradually larger, whereas their number became smaller, at the later stages of embryogenesis in the absence of *Nanos2* (Fig. 2*A–D*). This was also observed in *Nanos2, Bax* double-null male gonocytes (Fig. 2 *E* and *F*), where apoptotic cell death was suppressed, suggesting that apoptosis does not affect P-body status. This indicates that NANOS2 is not essential for the assembly of P-bodies but is required for the maintenance of their normal state. To further elucidate the functions of NANOS2 in P-body formation, we also examined the status of the P-bodies in NANOS2-expressing female gonocytes (6). Although they could not be detected in normal female gonocytes at E16.5, we found many P-bodies in NANOS2-expressing female cells and additionally observed that NANOS2 localizes at the P-bodies in these cells (Fig. 2 *G–I*). These data indicate that NANOS2 is sufficient to maintain the number of P-bodies when female gonocytes have acquired a male-type phenotype due to NANOS2 expression.

NANOS2 Interacts with the CCR4-NOT Deadenylation Complex and Regulates Its Localization. To explore the molecular functions of NANOS2, we searched for proteins that interact with it. To this end, we prepared male gonadal extracts from *Nanos2*$^{+/-}$ and *Nanos2*$^{-/-}$ embryos at E14.5 and subjected them to immunoprecipitation with anti-NANOS2 antibodies. We found that two major bands of more than 200 kDa were exclusively precipitated from *Nanos2*$^{+/-}$ gonads, and by mass spectrometric analysis identified these products as CNOT1, a component of the CCR4-NOT deadenylation complex (13) (Fig. 3A).

In further immunoprecipitation experiments, we used a transgenic mouse line expressing a FLAG-tagged NANOS2 under the direct control of the *Nanos2* enhancer (15) (Fig. S5*A*), since we had confirmed that this fusion protein was functional (Fig. S5 *B–F*) and localized at the P-bodies (Fig. S5 *G–I*). Western analyses revealed that CNOT1 coprecipitates with FLAG-tagged NANOS2 (Fig. 3*B, Upper*), confirming the results of our mass spectrometric analysis. We also found that other components of the CCR4-NOT complex, CNOT3, CNOT6L/Ccr4b, CNOT7/Caf1a, and CNOT9/Rcd1 (13, 21), also coprecipitated with FLAG-tagged NANOS2, indicating that NANOS2 associates with the CCR4-NOT deadenylation complex in vivo. We additionally found that this interaction is independent of RNA, as the levels of coprecipitated CNOT proteins were not affected by treatments with RNase (Fig. 3*B*). Finally, these CNOT proteins were found to colocalize with NANOS2 in P-bodies (Fig. 3 *C–E* and Fig. S6 *A–I*), suggesting that this complex may play a role in the activities of these elements.

To better understand the physiological significance of its interaction with NANOS2, we investigated the localization of CCR4-NOT deadenylation complex in *Nanos2*$^{-/-}$ male gonads by immunostaining CNOT proteins with DCP1A, another decapping enzyme and also a component of P-bodies (13, 14). Although CNOT3 was found to clearly localize to P-bodies in *Nanos2*$^{+/-}$ male gonads (Fig. 3 *F–H*), we detected only weak signals for this protein in P-bodies in the absence of NANOS2 (Fig. 3 *I–K*) even though the levels of CNOT3 are not reduced in *Nanos2*$^{-/-}$ male gonads (Fig. 3*L*). We obtained similar results for CNOT1 (Fig. S7). These data suggest that NANOS2 promotes the localization of the CCR4-NOT deadenylation complex to P-bodies, although a subpopulation of this complex still remains in these structures in the absence of NANOS2, possibly via a NANOS2-independent mechanism. Based on these findings and the fact that the CCR4-NOT deadenylation complex regulates the first step of mRNA degradation (22), we speculate that NANOS2 recruits this deadenylation complex to P-bodies where it promotes the degradation of RNAs.

Complex of NANOS2 and CCR4-NOT Deadenylation Complex in Male Germ Cells Retains Deadenylase Activity. To address the critical question of whether NANOS2-interacting deadenylase actually has catalytic activity, we used NANOS2-overexpressing (NANOS2 O/E) adult testes to obtain sufficient amounts of this protein and thus overcome the limitations of using embryonic testis in biochemical analyses. In the testis of the postnatal mouse, NANOS2 is expressed in a small population of undifferentiated spermatogonia (23) and localizes to P-bodies (Fig. S8 *A–C*) as in the male gonocytes. This expression is subsequently lost as these cells differentiate. However, if FLAG-tagged NANOS2 is forcedly and continuously expressed in the spermatogonial population, the male mouse become infertile because the spermatogonia remain in an undifferentiated state in the testis, in which a large number of NANOS2-positive spermatogonia occupy the periphery of the seminiferous tubules (23). In addition, FLAG-tagged NANOS2 also localizes to the P-bodies in the spermatogonia in the manner similar to endogenous Nanos2 (Fig. S8 *D–F*). We prepared testis extracts from this mouse and performed immunoprecipitations with anti-FLAG antibodies and control IgG, and then subjected these immunoprecipitates to in vitro deadenylase assay (21) (Fig. 4*A*). As shown in Fig. 4*B*, cleavage of the poly(A) RNA substrate occurred only with NANOS2 immunoprecipitates, which also contains the CNOT6L and CNOT7 catalytic components of the deadenylation complex (Fig. 4*C*). These results lead us to propose that NANOS2 promotes the degradation of NANOS2-interacting mRNAs through the deadenylase activity of the CCR4-NOT complex.

NANOS2 Interacts with Specific mRNAs and May Promote Their Degradation. Based on our working hypothesis, we further speculated that (*i*) the NANOS2 complex should contain specific mRNAs that would be degraded via NANOS2-mediated deadenylation, such that (*ii*) the expression levels of these transcripts would be low in wild-type male gonocytes but up-regulated in the absence of NANOS2. To test these possibilities, RNAs that coprecipitated with FLAG-tagged NANOS2 were purified and subjected to RT-PCR. Because we had previously shown that male gonocytes could enter meiosis in the absence of NANOS2, it was plausible that mRNAs involved in meiosis might be directly suppressed through NANOS2-mediated RNA degradation. As expected, *Sycp3*, *Stra8*, *Taf7l*, *Dazl*, and *Meisetz* (3, 24–27) transcripts that are implicated in meiosis were specifically detected only in the NANOS2 protein precipitates despite their very low expression in male gonads (Fig. 5 *A* and *B*). In contrast, the

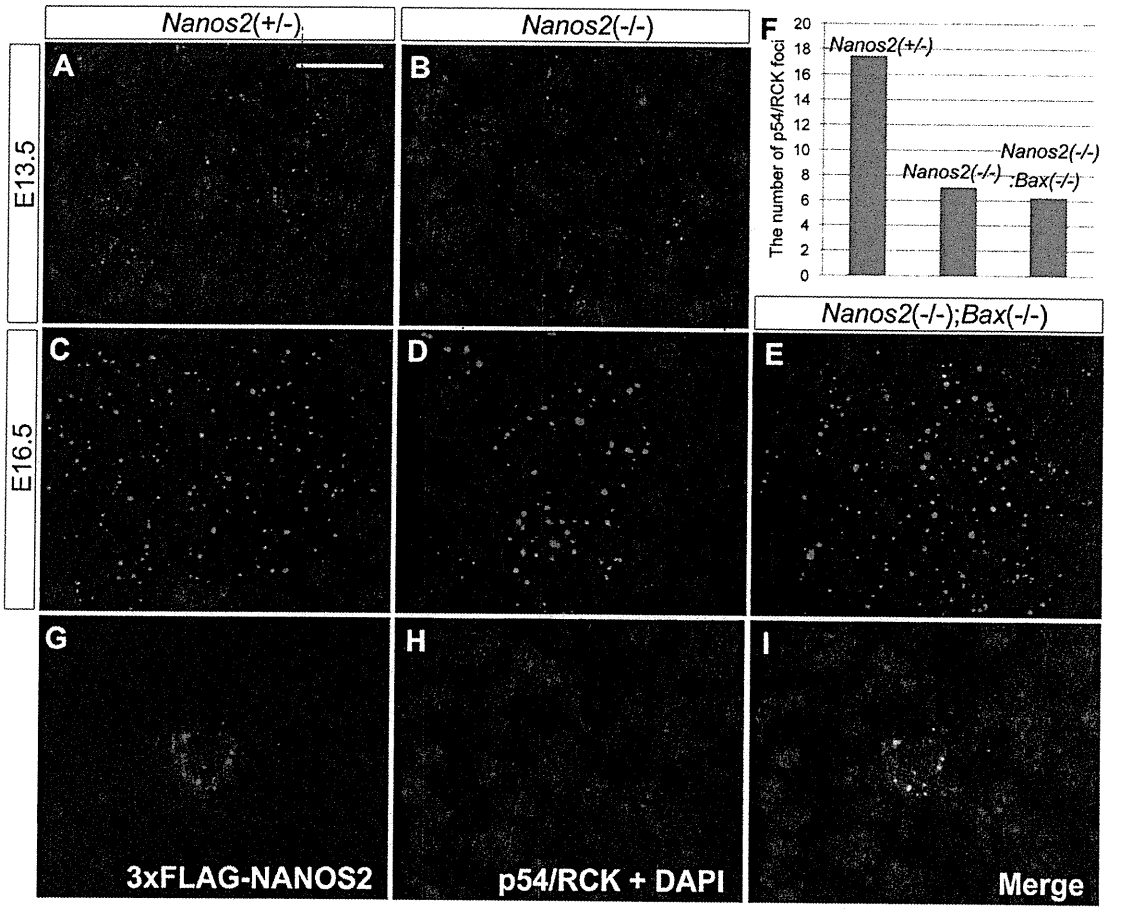

Fig. 2. Functional role of NANOS2 during the formation of the P-bodies. (*A–E*) Male gonadal sections from *Nanos2*$^{+/-}$ (*A* and *C*), *Nanos2*$^{-/-}$ (*B* and *D*), and *Nanos2*$^{-/-}$*Bax*$^{-/-}$ (*E*) embryos at stages E13.5 (*A* and *B*), and E16.5 (*C, D,* and *E*) were immunostained with p54/RCK (green) and TRA98 (red) antibodies. (*F*) Average number of p54/RCK foci per male gonocyte at E16.5 was quantified in each picture using ImageJ software (National Institutes of Health) and a cell counter, with the foci of less than a 20 permission value excluded using Photoshop (Adobe). The data shown correspond to two to three pictures. (*G–I*) A female gonadal section from a NANOS2-expressing embryo at E16.5 was immunostained with anti-FLAG (green) (*G*) and anti-p54/RCK (red) (*H*) antibodies. DNA was counterstained using DAPI (blue). (Scale bar in *A,* 20μm for *A–E* and *G–I.*)

G3pdh, *Dnmt3l* and *Dnmt3a* mRNAs did not show specific accumulation in the NANOS2 precipitates although they are all highly expressed in male gonads. These data indicate that the mRNAs involved in meiosis specifically interact with NANOS2 in vivo.

We next investigated global changes in gene expression upon the loss of *Nanos2* using comparative GeneChip analyses (Table S1). The resulting scatter plots showed that many genes become up- or down-regulated in *Nanos2*$^{-/-}$ male gonads by E15.5 (Fig. S9 *A–C*). For example, we found that the genes highly expressed only in male gonocytes, such as *Dnmt3l*, *Tdrd1* and *Miwi2*/*Piwi-like 4* (19, 28, 29), are down-regulated in the *Nanos2*$^{-/-}$ male gonads, whereas *Figla*, *Lhx8* and *Nobox*, which have been shown to be essential only for oogenesis and not for spermatogenesis (30–32), become accumulated in the *Nanos2*$^{-/-}$ male gonads (6) (Fig. S9 *D–I*). These results suggest that male gonocytes cannot enter the male pathways and become feminized by the up-regulation of female-type genes. In addition, and consistent with the results of our immunoprecipitation assay, *Sycp3*, *Stra8*, *Taf7l*, *Dazl,* and *Meisetzs* mRNAs were also found to be up-regulated in *Nanos2*$^{-/-}$ male gonads (Fig. 5 *C–G*). Our current findings thus indicate that NANOS2-interacting mRNAs become accumulated if NANOS2 is absent in male gonocytes, which in turn indicates that NANOS2 might be indirectly affecting the transcription of these genes, or that they are normally suppressed in wild-type male gonocytes through a NANOS2-directed mechanism, possibly a deadenylation pathway.

Discussion

Molecular Role of NANOS2. In our current study, we show that the CCR4-NOT deadenylation complex is coprecipitated with NANOS2 from male gonadal extracts. This is the first evidence that the interaction between a Nanos homolog and the CCR4-NOT deadenylation complex exists *in vivo,* although it has been shown using a yeast two-hybrid system that *Drosophila* Nanos can directly and potently bind to NOT4, a component of the CCR4-NOT complex (33). Hence, as suggested previously by Kadyrova et al. for *Drosophila* Nanos, and as confirmed by our present analyses in vivo, the recruitment of the CCR4-NOT deadenylation complex to target mRNAs may be a conserved function of the Nanos proteins.

We also found that NANOS2 localizes to P-bodies in the male gonocytes and adult mouse spermatogonia. P-bodies are known to be a central hub of RNA degradation, in which decapping enzymes and exonucleases are also localized. However, emerging evidence in other systems suggests that P-bodies not only function to degrade RNAs but also to store mRNAs in a translationally quiescent state until needed (13). In addition, *Drosophila* Nanos promotes the deadenylation of poly(A) tail in *hunchback* mRNA and represses its translation without changing the mRNA level

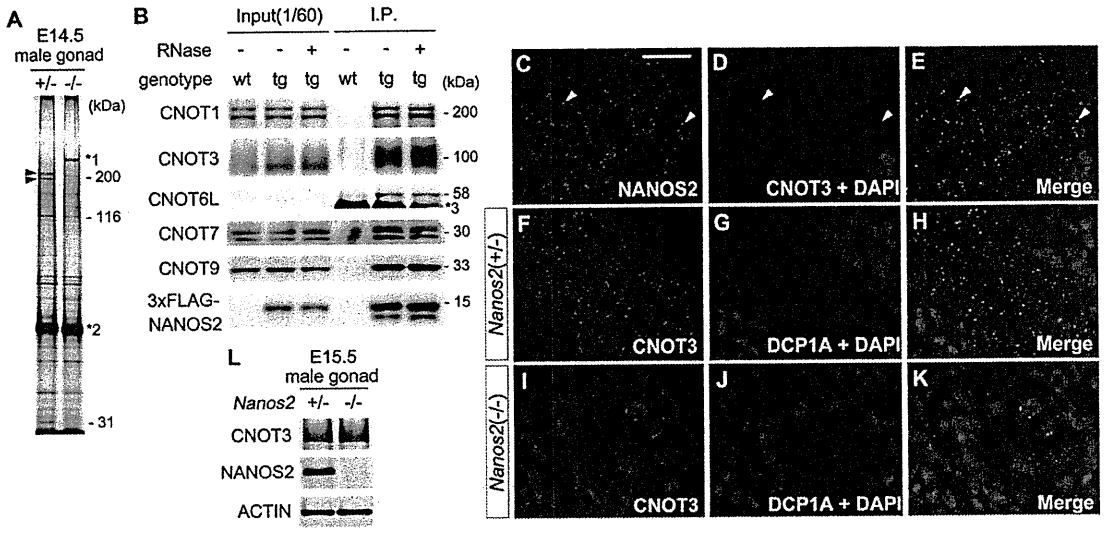

Fig. 3. Interaction between NANOS2 and the CCR4-NOT deadenylation complex. (*A*) Proteins coimmunoprecipitated with NANOS2 from E14.5 wild-type (lane 1) and *Nanos2*$^{-/-}$ (lane 2) male gonadal extracts using rabbit anti-NANOS2 antibodies. Arrowheads indicate CNOT1. *1, nonspecific band; *2, IgG polypeptide. (*B*) Immunoprecipitation–Western blot analyses of proteins from male gonadal extracts of wild-type and transgenic embryos expressing 3×FLAG-NANOS2. *3, IgG polypeptide from the anti-FLAG antibody. (*C–E*) Male gonadal sections from E15.5 embryos were immunostained with mouse NANOS2 (green) (*C*) and CNOT3 (red) (*D*) antibodies. Arrowheads in *C–E* indicate colocalization between NANOS2 and CNOT3. (*F–K*) Male gonadal sections from *Nanos2*$^{+/-}$ (*F–H*) and *Nanos2*$^{-/-}$ (*I–K*) embryos at E15.5 were immunostained with DCP1A (red) (*G* and *J*) and CNOT3 (green) (*F* and *I*) antibodies. DNA was labeled via DAPI counterstaining (blue). (*L*) Western blot analyses of proteins from the male gonads of *Nanos2*$^{+/-}$ and *Nanos2*$^{-/-}$ embryos at E15.5.

(34). We cannot therefore rule out the possibility that NANOS2 not only promotes the degradation of mRNAs involved in meiosis but also retains other transcripts at P-bodies to sequester them in a translationally inactive state during embryogenesis. These transcripts may be released from the P-bodies and translated to promote differentiation after birth as NANOS2 expression begins to disappear.

P-Body Formation in Male Mouse Gonocytes. P-bodies have been well characterized in yeast and mammalian cultured cells, and the in vivo status of these foci has begun to be described recently also in worms and flies (35–38). We found from our current analyses that P-bodies are specifically formed and/or maintained in the germ cells of male mouse embryonic gonads, whereas no such structures are detectable in somatic cells. Furthermore, female mouse gonocytes fail to maintain P-bodies at later stages of embryogenesis. We thus suggest that P-bodies play roles in cell-type specific differentiation during mouse development through RNA metabolism.

It has also been shown that P-bodies are dynamic structures and that their size and number reflects the status of the mRNA supply. If the transit of mRNAs into the P-bodies is inefficient, the size and number of these structures becomes extremely small. In contrast, they become larger when the mRNA decapping pathway is blocked (39, 40). Furthermore, it has been recently reported that deadenylation is required for P-body formation (41). Taking into account the data presented in these earlier reports and our current model, P-bodies would be expected to be small in *Nanos2*$^{-/-}$ male gonocytes because the mRNA supply to these structures and subsequent deadenylation efficiency would be inhibited in the absence of NANOS2. However, we were surprised to find that the sizes of the P-bodies

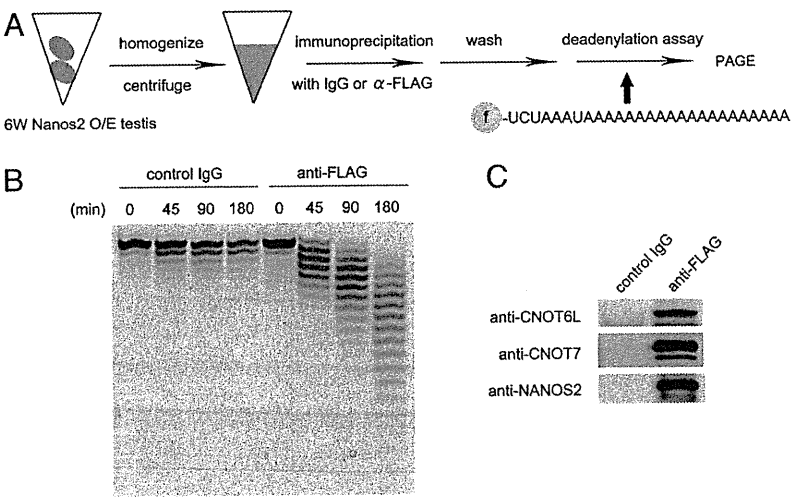

Fig. 4. The protein complex of NANOS2 and CCR4-NOT complex has in vitro deadenylase activity. (*A*) Schematic representation of the in vitro deadenylase assay method using NANOS2 over-expressing (O/E) testes. (*B*) FLAG-tagged NANOS2 was precipitated with anti-FLAG antibodies from the testis extracts of a 6-week-old NANOS2 O/E mouse and incubated with 5′-fluorescein isothiocyanate-labeled poly (A) RNA substrate for 0, 45, 90, and 180 min. Samples were then analyzed on a denaturing sequencing gel, as previously described (**21**) (*G*). (*C*) Western blot analyses reveaing that CNOT6L and CNOT7 are coprecipitated with FLAG-tagged NANOS2.

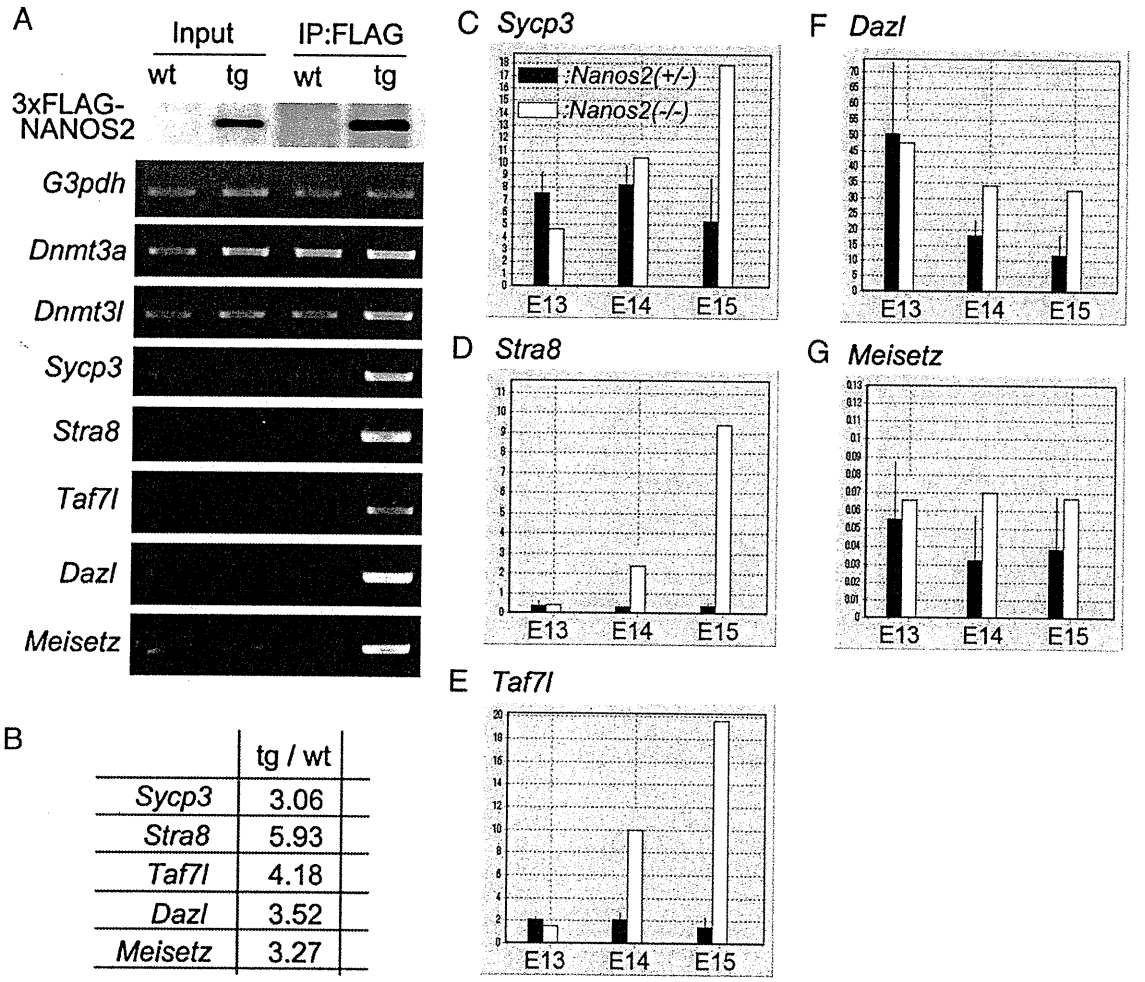

B

	tg / wt
Sycp3	3.06
Stra8	5.93
Taf7l	4.18
Dazl	3.52
Meisetz	3.27

Fig. 5. NANOS2 interacts with specific mRNAs and may promote their degradation. (*A*) Male gonadal extracts from wild-type (*wt*) and transgenic (*tg*) mice expressing FLAG-NANOS2 at E15.5 were subjected to immunoprecipitation (IP) with FLAG antibodies. RNA precipitates were analyzed by semi-quantitative RT-PCR. (*B*) Quantification of each mRNA enrichment from a FLAG IP of *tg* extracts using real-time RT-PCR. Fold enrichment of each mRNA coprecipitated from *tg* compared with those from *wt* is indicated. Mean value of three independent QRT-PCR results is shown. (*C–G*) Expression profiling of the *Sycp3* (*C*), *Stra8* (*D*), *Taf7l* (*E*), *Dazl* (*F*), and *Meisetz* (*G*) genes in male gonads from *Nanos2*$^{+/-}$ and *Nanos2*$^{-/-}$ embryos at E13.5-E15.5 using the Affymetrix GeneChip System as previously described (43) (*X*-axis; embryonic stage, *Y*-axis; expression level, black bars; *Nanos2*$^{+/-}$ embryos, white bars; *Nanos2*$^{-/-}$ embryos).

became larger in this biological context, although their number was decreased. These data thus indicate that male gonocytes have a unique program for P-body formation that occurs both in a NANOS2-dependent and -independent manner.

mRNAs Targeted by NANOS2. We elucidated that the protein complex of NANOS2 and CCR4-NOT complex has deadenylase activity in vitro. We thus expected that the poly(A) tail lengths of NANOS2-interacting mRNAs would be maintained without NANOS2. To test this scenario, we assayed the poly(A) tail length of NANOS2-interacting mRNAs. However, we could not observe clear shortening of the poly(A) tail in wild-type male gonads, possibly because of their low abundance. New experimental systems will be required in the future to address this issue.

On the other hand, it was noteworthy that we identified *Stra8* as a NANOS2-interacting mRNA because we have shown previously that *Stra8* is up-regulated at the transcriptional level in *Nanos2*$^{-/-}$ male gonocytes (6). These data together indicate that the suppression of *Stra8* in male gonocytes is ensured at both the transcriptional and translational levels, suggesting the critical functional importance of suppressing this gene during male gonocyte development.

Materials and Methods

Mice. Both the *Nanos2* and *Bax*-knockout mouse lines and PCR methods used for the verification of each mutant allele have been previously described (11, 42). The NANOS2-expressing mouse line has also been described (23) The transgene containing 3×FLAG-tagged *Nanos2* with the 3′-UTR under the control of Nanos2 enhancer (9.2 kb upstream sequence) was used for the production of the transgenic mouse line.

Histological Methods. For immunostaining, mouse gonads of both sexes were directly embedded in O.C.T. compound (Sakura) and frozen in liquid nitrogen. After sectioning (8 μm), samples were stained according to standard procedures.

Immunoprecipitation. Extracts of male gonads from E14.5 or E15.5 embryos were incubated with protein-A beads crosslinked with rabbit anti-NANOS2 antibody or anti-FLAG M2 affinity gel (Sigma).

In Vitro Deadenylase Assay. The testis extracts from NANOS2-expressing mice were incubated with anti-FLAG M2 affinity gel or Mouse IgG-agarose (Sigma). After several washes, precipitates were then subjected to a deadenylase assay as previously described (21).

RT-PCR. After synthesis of first-strand cDNAs with SuperScript III reverse transcriptase and $(dT)_{20}$ primer (Invitrogen), PCR analyses were carried out either using a regular or real-time protocol.

GeneChip Analysis. Total RNAs were purified from cells corresponding to the male gonads of *Nanos2-LacZ* knock-in heterozygous and homozygous embryos, and analyzed using a GeneChip Mouse Genome 430 2.0 Array (Affymetrix).

Details of the methods and primer sequences used for each section are provided in *SI Text*.

ACKNOWLEDGMENTS. We thank the following researchers for generously providing antibodies: Y. Nishimune (TRA98), S. Chuma and N. Nakatsuji (anti-TDRD1), T. Noce (anti-MVH), M. Kiledjian (anti-hDCP2), W. D. Heyer (anti-mXRN1), H. T. Timmers (anti-CNOT1), T. Tamura (anti-CNOT3), T. Yamamoto (anti-CNOT6L/Ccr4b), A. B. Shyu (anti-CNOT7/Caf1a), and H. Okayama (anti-CNOT9/Rcd1). We are also very grateful to M. Morita and T. Yamamoto for their technical advice and assistance with the *in vitro* deadenylase assay. We further thank Noriko Moriyama for technical assistance with the microarray experiments and Yuki Nakajima for help with the histological analyses. This work was partly supported by Grants-in-Aid for National BioResource Project and of the Genome Network Project of the Ministry of Education, Culture, Sports, Science and Technology, Japan.

1. Hayashi K, de Sousa Lopes SM, Surani MA (2007) Germ cell specification in mice. *Science* 316:394–396.
2. Bowles J, Koopman P (2007) Retinoic acid, meiosis and germ cell fate in mammals. *Development* 134:3401–3411.
3. Baltus AE, et al. (2006) In germ cells of mouse embryonic ovaries, the decision to enter meiosis precedes premeiotic DNA replication. *Nat Genet* 38:1430–1434.
4. Bowles J, et al. (2006) Retinoid signaling determines germ cell fate in mice. *Science* 312:596–600.
5. Koubova J, et al. (2006) Retinoic acid regulates sex-specific timing of meiotic initiation in mice. *Proc Natl Acad Sci USA* 103:2474–2479.
6. Suzuki A, Saga Y (2008) Nanos2 suppresses meiosis and promotes male germ cell differentiation. *Genes Dev* 22:430–435.
7. Kobayashi S, Yamada M, Asaoka M, Kitamura T (1996) Essential role of the posterior morphogen nanos for germline development in Drosophila. *Nature* 380:708–711.
8. Murata Y, Wharton RP (1995) Binding of pumilio to maternal hunchback mRNA is required for posterior patterning in Drosophila embryos. *Cell* 80:747–756.
9. Asaoka-Taguchi M, Yamada M, Nakamura A, Hanyu K, Kobayashi S (1999) Maternal Pumilio acts together with Nanos in germline development in Drosophila embryos. *Nat Cell Biol* 1:431–437.
10. Sato K, et al. (2007) Maternal Nanos represses hid/skl-dependent apoptosis to maintain the germ line in Drosophila embryos. *Proc Natl Acad Sci USA* 104:7455–7460.
11. Tsuda M, et al. (2003) Conserved role of nanos proteins in germ cell development. *Science* 301:1239–1241.
12. Suzuki H, Tsuda M, Kiso M, Saga Y (2008) Nanos3 maintains the germ cell lineage in the mouse by suppressing both Bax-dependent and -independent apoptotic pathways. *Dev Biol* 318:133–142.
13. Parker R, Sheth U (2007) P bodies and the control of mRNA translation and degradation. *Mol Cell* 25:635–646.
14. Eulalio A, Behm-Ansmant I, Izaurralde E (2007) P bodies: At the crossroads of post-transcriptional pathways. *Nat Rev Mol Cell Biol* 8:9–22.
15. Suzuki A, Tsuda M, Saga Y (2007) Functional redundancy among Nanos proteins and a distinct role of Nanos2 during male germ cell development. *Development* 134:77–83.
16. Hay B, Ackerman L, Barbel S, Jan LY, Jan YN (1988) Identification of a component of Drosophila polar granules. *Development* 103:625–640.
17. Bardsley A, McDonald K, Boswell RE (1993) Distribution of tudor protein in the Drosophila embryo suggests separation of functions based on site of localization. *Development* 119:207–219.
18. Toyooka Y, et al. (2000) Expression and intracellular localization of mouse Vasa-homologue protein during germ cell development. *Mech Dev* 93:139–149.
19. Chuma S, et al. (2003) Mouse Tudor Repeat-1 (MTR-1) is a novel component of chromatoid bodies/nuages in male germ cells and forms a complex with snRNPs. *Mech Dev* 120:979–990.
20. Kedersha N, Anderson P (2007) Mammalian stress granules and processing bodies. *Methods Enzymol* 431:61–81.
21. Morita M, et al. (2007) Depletion of mammalian CCR4b deadenylase triggers elevation of the p27Kip1 mRNA level and impairs cell growth. *Mol Cell Biol* 27: 4980–4990.
22. Meyer S, Temme C, Wahle E (2004) Messenger RNA turnover in eukaryotes: Pathways and enzymes. *Crit Rev Biochem Mol Biol* 39:197–216.
23. Sada A, Suzuki A, Suzuki H, Saga Y (2009) The RNA-binding protein NANOS2 is required to maintain murine spermatogonial stem cells. *Science* 325:1394–1398.
24. Yuan L, et al. (2000) The murine SCP3 gene is required for synaptonemal complex assembly, chromosome synapsis, and male fertility. *Mol Cell* 5:73–83.
25. Cheng Y, et al. (2007) Abnormal sperm in mice lacking the Taf7l gene. *Mol Cell Biol* 27:2582–2589.
26. Ruggiu M, et al. (1997) The mouse Dazla gene encodes a cytoplasmic protein essential for gametogenesis. *Nature* 389:73–77.
27. Hayashi K, Yoshida K, Matsui Y (2005) A histone H3 methyltransferase controls epigenetic events required for meiotic prophase. *Nature* 438:374–378.
28. Sakai Y, Suetake I, Shinozaki F, Yamashina S, Tajima S (2004) Co-expression of de novo DNA methyltransferases Dnmt3a2 and Dnmt3L in gonocytes of mouse embryos. *Gene Expr Patterns* 5:231–237.
29. Aravin AA, et al. (2008) A piRNA pathway primed by individual transposons is linked to de novo DNA methylation in mice. *Mol Cell* 31:785–799.
30. Soyal SM, Amleh A, Dean J (2000) FIGalpha, a germ cell-specific transcription factor required for ovarian follicle formation. *Development* 127:4645–4654.
31. Choi Y, Ballow DJ, Xin Y, Rajkovic A (2008) Lim homeobox gene, lhx8, is essential for mouse oocyte differentiation and survival. *Biol Reprod* 79:442–449.
32. Rajkovic A, Pangas SA, Ballow D, Suzumori N, Matzuk MM (2004) NOBOX deficiency disrupts early folliculogenesis and oocyte-specific gene expression. *Science* 305: 1157–1159.
33. Kadyrova LY, Habara Y, Lee TH, Wharton RP (2007) Translational control of maternal Cyclin B mRNA by Nanos in the Drosophila germline. *Development* 134:1519–1527.
34. Wreden C, Verrotti AC, Schisa JA, Lieberfarb ME, Strickland S (1997) Nanos and pumilio establish embryonic polarity in Drosophila by promoting posterior deadenylation of hunchback mRNA. *Development* 124:3015–3023.
35. Boag PR, Atalay A, Robida S, Reinke V, Blackwell TK (2008) Protection of specific maternal messenger RNAs by the P body protein CGH-1 (Dhh1/RCK) during Caenorhabditis elegans oogenesis. *J Cell Biol* 182:543–557.
36. Gallo CM, Munro E, Rasoloson D, Merritt C, Seydoux G (2008) Processing bodies and germ granules are distinct RNA granules that interact in C. elegans embryos. *Dev Biol* 323:76–87.
37. Noble SL, Allen BL, Goh LK, Nordick K, Evans TC (2008) Maternal mRNAs are regulated by diverse P body-related mRNP granules during early Caenorhabditis elegans development. *J Cell Biol* 182:559–572.
38. Lee L, Davies SE, Liu JL (2009) The spinal muscular atrophy protein SMN affects Drosophila germline nuclear organization through the U body-P body pathway. *Dev Biol* 332:142–155.
39. Sheth U, Parker R (2003) Decapping and decay of messenger RNA occur in cytoplasmic processing bodies. *Science* 300:805–808.
40. Eulalio A, Behm-Ansmant I, Schweizer D, Izaurralde E (2007) P-body formation is a consequence, not the cause, of RNA-mediated gene silencing. *Mol Cell Biol* 27: 3970–3981.
41. Zheng D, et al. (2008) Deadenylation is prerequisite for P-body formation and mRNA decay in mammalian cells. *J Cell Biol* 182:89–101.
42. Knudson CM, Tung KS, Tourtellotte WG, Brown GA, Korsmeyer SJ (1995) Bax-deficient mice with lymphoid hyperplasia and male germ cell death. *Science* 270: 96–99.
43. Kanno J, et al. (2006) "Per cell" normalization method for mRNA measurement by quantitative PCR and microarrays. *BMC Genomics* 7:64.

ENVIRONMETRICS
Environmetrics 2009; **20**: 1–13
Published online 8 May 2008 in Wiley InterScience
(www.interscience.wiley.com) DOI: 10.1002/env.898

An experimental design for judging synergism on consideration to endocrine disruptor animal experiments

Nobuhito Matsunaga[1*,†], Jun Kanno[2], Chikuma Hamada[3] and Isao Yoshimura[3]

[1]*Kyowa Pharmaceutical, Inc., 212 Carnegie Center, Suite 101, Princeton, NJ 08540, USA*
[2]*National Institute of Health Sciences, Tokyo, Japan*
[3]*Tokyo University of Science, Tokyo, Japan*

SUMMARY

This paper investigates an appropriate statistical design for an animal experiment to evaluate synergism of two test chemicals. It assumes a certain number of animals are divided into groups, each of which is treated with a combination of dose levels of two chemicals. A design is identified by the set of group size for each combination of doses, including the case where the dose of either one chemical is zero. The power of t-test to detect synergism by positive surplus of response on a simultaneous administration group from the additivity plane composed of the responses on single administration groups is adopted as the criterion for the appropriate design. The applicable design is investigated for the application to real cases of endocrine disrupter study conducted at the National Institute of Health Sciences of Japan.

It revealed that the dose level of the simultaneous administration group should be located inside or on the boundary of a triangular region and that the total number of animals should be the same as those for single administration groups. Copyright © 2008 John Wiley & Sons, Ltd.

KEY WORDS: additivity; animal experiment; experimental design; endocrine disruptor; synergism; triangular region

1. INTRODUCTION

In the past, environmental pollutants were regulated according to individual effects. However, recently, there has arisen the problems of combinations of complex pollutants, and regulations that address synergism have become necessary. As a result, experimental researches have been conducted on pollutant synergism. The investigation by Kanno, one of the authors (Kanno *et al.*, 2001) on the synergism of endocrine disruptors, using the rodent uterotrophic assay, is an example of such researches.

In our experiments using multiple test substances, dividing animals such as rats into multiple groups of single administration and simultaneous administration, we estimated the response when there is no synergism based on the response in the single administration group to investigate whether the response in the simultaneous administration group exceeds the estimated response.

*Correspondence to: N. Matsunaga, Kyowa Pharmaceutical, Inc., 212 Carnegie Center, Suite 101, Princeton, NJ 08540, USA.
†E-mail: matsunaga.nobuhito@kyowa-kpi.com

Received 21 February 2006
Accepted 20 October 2007